

## Summary

*An investigation has been conducted in the Langley 16-Foot Transonic Tunnel to determine boundary-reflected disturbance lengths at low supersonic Mach numbers in the octagonally shaped test section. A body of revolution that had a nose designed to produce a bow shock and flow field similar to that about the nose of a supersonic transport configuration was used. The impingement of reflected disturbances on the model was determined from static pressures measured on the surface of the model. Test variables included Mach number (0.90 to 1.25), model angle of attack (nominally  $-10^\circ$ ,  $0^\circ$ , and  $10^\circ$ ), and model roll angle.*

*Results showed that the body, which had a blockage ratio of 0.000575, experienced interference associated with the reflection of the expansion field generated by the forward portion of the model at the lower supersonic Mach numbers. The model lengths that would be free of the bow-shock boundary-reflected disturbance were determined at Mach numbers from 1.03 to 1.08. When compared to bow-shock reflection lengths previously obtained on cone-cylinder bodies, it was found that the effect of the large nose initial-half-angle (approximately  $15^\circ$ ) on reflection-free length was lessened by the continuously decreasing local body half angle downstream of the nose. The variation of reflection-free length with Mach number was fairly linear and showed essentially the same trend as cone-cylinder data. Model angle of attack did not affect the reflected-disturbance impingement point on the model since the center of rotation for angle of attack was approximately the midpoint of the model. When the model was rolled to direct the closely-spaced row of pressure orifices towards a test section slot no difference in pressure distributions was observed. Mach number 1.05 was set with and without the use of test section plenum suction and it was found that flow removal from the test section through the slots did not affect boundary conditions enough to be evident in reflection-free model lengths.*

## Introduction

There are several factors related to model size that must be considered if valid data is to be obtained from a transonic wind tunnel test. Depending on the particular Mach number range of interest for a given investigation any or all of three factors must be considered before a model is built or a commitment is made to a test plan. The first is model position in the test section; that is, ensuring that the model is located completely within the calibrated portion of the test section at all the Mach numbers of interest. The second is test section blockage ratio; that is, ensuring that the model maximum cross-sectional area/test section area ratio is small enough so that essentially blockage-free data can be obtained at the highest subsonic Mach number planned for the investigation. And the third concerns model length; that is, ensuring that the model is of appropriate length to avoid impingement of wall-reflected disturbances at the lowest supersonic Mach number of the investigation. The calibration data necessary to allow decisions to be made on the appropriateness of a certain size model for an investigation is unique to each wind tunnel and is often sparse or incomplete especially regarding shock reflection length since it depends to

some extent on the details of the model geometry. As time passes the need for more detail of tunnel capability in specific areas necessitates additional calibrations. This need forms the impetus for the present investigation in which data was obtained on boundary-reflected disturbance lengths in the Langley 16-Foot Transonic Tunnel for a sharp-nosed body of revolution at low supersonic Mach numbers.

The Langley 16-Foot Transonic Tunnel is a closed-circuit single-return atmospheric wind tunnel that has a slotted transonic test section with a Mach number range from 0.1 to 1.3. The test section is octagonal in shape and has longitudinal slots at the wall vertices. It is fan driven but also uses test-section plenum suction for Mach numbers of 1.05 and above. Because of the large test-section cross-sectional area it is possible to test small models (with less instrumentation) to higher subsonic Mach numbers than smaller tunnels before significant blockage effects are encountered. In addition, the large test section diameter permits testing of a given model to lower supersonic Mach numbers (closer to Mach 1.0) than smaller slotted tunnels before nose-originated shocks are reflected by the test section boundary and impinge as disturbances on the model. As the facility has been modified and upgraded over the years it has been recalibrated periodically to validate and

document its expanded capabilities. An overview of the tunnel developmental history, its capabilities, and detailed current calibrations are contained in reference 1. Additional tunnel calibrations are conducted as necessary for specific tests or as part of comparison surveys with other transonic facilities.

The present investigation was conducted as part of a survey of three wind tunnels to determine the impingement location at low supersonic Mach numbers of wall-reflected disturbances originating as shocks at the nose of a body of revolution. The other two wind tunnels included in the survey were the Boeing Transonic Wind Tunnel (BTWT) and the Boeing Supersonic Wind Tunnel (BSWT). The nose of the body of revolution was designed to have a geometry that would produce a shock having the same strength as that of a supersonic transport configuration for which aerodynamic data was required in the supersonic speed range below Mach 1.1. The body downstream of the nose was designed to have nearly zero pressure coefficient along its length at a Mach number of 1.3. From these tests the lowest supersonic Mach number could be determined at which data free of wall-reflected disturbance impingement could be obtained for the specific model in each of the three tunnels. Impingement of wall-reflected disturbances on the body of revolution was determined from the abrupt changes in pressure measured by a closely-spaced longitudinal row of pressure orifices. Pressure distributions on the 64-inch long body in the 16-Foot Transonic Tunnel were obtained at Mach numbers from 0.90 to 1.25 and at angles of attack of about  $-10^\circ$ ,  $0^\circ$ , and  $10^\circ$ . This data complements boundary-reflected-disturbance length measurements previously made in the 16-Foot Transonic Tunnel on bodies of revolution with conical and ogive noses combined with cylindrical aft sections (ref. 2).

## Symbols

$C_p$	pressure coefficient
$d$	local model diameter, in.
$d_b$	model base diameter, 4.605 in.
$M$	Mach number
SRB	shock reflection body
$x$	distance measured from tip of nose aft, in.
TS	tunnel station, ft
$\alpha$	model angle of attack (measured in vertical plane of test section), deg
$\delta$	test section wall divergence angle, deg

$\phi$  angular location of orifices on model, positive clockwise, deg

$\phi_m$  model roll angle, positive clockwise, deg

## Wind Tunnel

The investigation was conducted in the Langley Research Center 16-Foot Transonic Tunnel which is a single-return atmospheric wind tunnel with continuous air exchange. The test section is octagonal in shape with 15.5 feet between the centerlines of opposite walls (equivalent in area to a circle 16 feet in diameter) and has axial slots at the wall vertices. The total width of the eight slots in the vicinity of the model is approximately 3.7 percent of the test section perimeter. The eight flat segments that comprise the tunnel wall are remotely actuated and their divergence angle can be changed while the tunnel is operating to configure the test section for its optimum calibrated flow quality at each Mach number. To obtain Mach numbers of 1.05 and above an auxiliary system provides suction at the outer wall of the test section plenum and the air removed is exhausted to the atmosphere.

The tunnel arc-sector sting-support system pivots in the vertical plane (pivot point at TS 134.0) in such a manner that the model remains on or near the test section centerline through the angle of attack range if the model is installed in the appropriate longitudinal position. A roll coupling is incorporated in the sting support portion of the arc sector so that the model can be rolled about its axis of symmetry (centerline of the test section at  $\alpha = 0^\circ$ ) without shutting down the tunnel. Since the tunnel continually exchanges air with the atmosphere for cooling (20% per circuit) the flow in the freestream is subject to the daily atmospheric variations in ambient conditions. The tunnel has been calibrated at a number of ambient temperature and humidity conditions and essentially uniform centerline Mach number distributions are obtained at Mach numbers up to 1.1 by setting the test section walls at specific divergence angles regardless of ambient conditions. At Mach numbers above 1.1 it has been found that uniform centerline Mach number distributions are obtained at specific wall divergence angles for specific dew point conditions. The ranges of wall divergence angle set for the range of Mach numbers of this investigation are presented in table 1. Details of the tunnel history, operation, and flow qualities are presented in reference 1.

## Model

The 64-inch-long axisymmetric model was designed to have a nose shape that produces a bow

shock of about the same strength as the nose of a realistic supersonic transport airplane configuration of the same scale. Photographs of the body of revolution installed in the 16 Foot Transonic Tunnel are presented in figure 1 and its longitudinal location in the test section is presented in figure 2. The contours of the mid- and aft-body portions of the model were designed using an iterative technique to have a free-air pressure coefficient of nearly zero along their length at a Mach number of 1.3. The nearly zero design pressure coefficient distribution along the model serves as a convenient reference for the detection of the abrupt changes in pressure coefficient that occur when test section wall-reflected disturbances impinge on the model. Only a limited amount of model geometric data is available for publication but from that it has been determined that the initial half angle of the nose was approximately  $15^\circ$  and the longitudinal curvature on the forward portion of the model resulted in a chordal half angle of  $5.48^\circ$  for the forward 11.750 inches of the model. The model had a maximum diameter at its base of 4.605 inches. Geometric details of the model, model sting, and the forward portion of the sting-adaptor are also shown in figure 2. The 101 tubes connected to the model pressure orifices exited the model base as a bundle (fig.1) and were routed aft externally to the pressure sensing modules which were in the top portion of the tunnel support system.

The anodized model was made of 2024-T3 aluminum and had a polished surface. A longitudinal row of 86 closely-spaced 0.02-inch diameter orifices were installed along the top ( $\phi = 0^\circ$ ) of the model ( $\phi_m = 0^\circ$ ). Additional pressure orifices were installed at angles of  $\phi = 90^\circ$ ,  $180^\circ$ , and  $270^\circ$  at 5 stations aft of the model nose (at  $x = 10, 20, 30, 45$ , and  $60$  inches). The locations of the pressure orifices aft of the nose when the model was upright in the test section are shown in table 2.

## Instrumentation

Model pressures were measured on four 32-port electronic pressure-scanning modules housed in the sting-support portion of the arc sector. The module transducers had a full-scale differential pressure range of  $\pm 15$  psi and the manufacturer's quoted worst case static accuracy was  $\pm 0.10$  percent of full scale. An additional installation effect on model pressure measurements results from the sensitivity of the pressure-scanning modules to temperature. The modules were housed in the sting-support portion of the tunnel arc sector which is within the freestream flow environment. Since the tunnel cooling is dependent on air exchange with the atmosphere, freestream temperature is a function of atmospheric conditions and will also

vary with Mach number and run time. To minimize the effect of temperature variations on pressure-scanning module accuracy known pressures were supplied to two ports of each module so that the modules could be recalibrated as needed while the tunnel was operating. Based on this approach the uncertainty of the measured pressure coefficients is estimated to be  $\pm 0.006$  at a Mach number of 0.90 and  $\pm 0.005$  at a Mach number of 1.2. Model angle of attack was measured by an accelerometer in the top of the model sting support system. A correction of  $0.1^\circ$  was made for test section upflow angle based on measurements made on similar models (ref. 1). No correction has been made to angle of attack for any small sting deflections that might have occurred due to model loads.

## Tests

The upright model ( $\phi_m = 0^\circ$ ) was tested in the Mach number range from 0.90 to 1.25 at an angle of attack of  $0^\circ$  with the closely-spaced row of pressure orifices facing the centerline of the top wall of the test section. At Mach numbers from 1.00 to 1.25 the model (at  $\phi_m = 0^\circ$  and  $90^\circ$ ) was also tested at angles of attack of approximately  $-10^\circ$  and  $10^\circ$ . At Mach numbers of 1.05, 1.15, and 1.25 the model was rolled ( $\phi_m$ ) in  $22.5^\circ$  increments to  $180^\circ$  to change the orientation of the closely-spaced row of pressure orifices relative to the flat wall segments of the test section periphery. The usual method of setting a Mach number of 1.05 includes the application of test section plenum suction to avoid operation of the fan drive at its maximum power. However, the tunnel is also calibrated for a Mach number of 1.05 to be set without plenum suction. Therefore the availability of these two calibrated methods of obtaining a Mach number of 1.05 allows the determination of the effect of plenum suction on the location of wall-reflected-disturbance impingement on the model. This was done with the model rolled  $90^\circ$  with the closely-spaced row of model orifices directed toward the centerline of the side wall of the test section. It is on this side of the tunnel (at about  $80^\circ$ ) at which the plenum suction is applied through a 10 foot diameter opening (butterfly valve).

Since this investigation was directly related to a test of a supersonic transport configuration in the 16-Foot Transonic Tunnel and the model nose geometry represented that of the airplane configuration it was decided to further replicate the flow field on the nose of the airplane model by duplicating the artificially fixed boundary layer transition location selected for the airplane model. The transition fixing strip was located 1.0 inch aft of

the tip of the nose and consisted of a 0.005-inch high row of 0.05-inch diameter disks spaced 0.1-inch apart around the body. Based on the maximum diameter of the model, which is at the base, the blockage ratio of the model in the test section (maximum model cross-sectional area/test section cross-sectional area) is 0.000575. This indicates that subsonic data for this model should be free of blockage effects up to a Mach number of 0.97 (ref. 1).

## Presentation of Results

The results of this investigation are presented graphically as variations of pressure coefficient with model length in figures 3 through 7. The data are generally plotted against the length  $x$  so that the dimensional location of boundary-reflected-disturbance impingement on the model can be determined directly. As a reference for the pressure distributions a dashed outline of the body shape is included along the  $x$ -axis in each plot. An example of the sensitivity of the pressure coefficient on either side of the reflected-shock impingement point on the model to tunnel Mach number setting at low supersonic Mach numbers is presented in figure 8.

A comparison of the experimental pressure coefficient distribution measured along the model at Mach number 1.25 with that calculated using the Boeing Company's computational fluid dynamics program TRANAIR is reproduced from reference 3 as figure 9. The nose shock reflection-free model lengths determined from the present investigation combined with the cone- and ogive-cylinder reflection-free lengths determined from previous 16-Foot Transonic Tunnel investigations (refs. 1 and 2) are presented in figure 10.

## Discussion of Results

### Pressure Coefficient Distributions at $\alpha = 0^\circ$

The pressure coefficient distributions along and around the body at  $0^\circ$  angle of attack are presented in figure 3. These data indicate that the model was aligned with the flow and on the tunnel centerline in that pressures at  $\phi = 0^\circ, 90^\circ, 180^\circ$ , and  $270^\circ$  at five model stations are within the range of the uncertainty of the pressure measurements. At Mach numbers from 0.90 to 0.98 the pressure coefficient distributions indicate that pressure on the nose recovers to essentially freestream static pressure ( $C_p = 0$ ) without overexpansion. However, at a Mach number of 1.00 there is an overexpansion on the forward portion of the model that recovers to stream conditions over a length of

about 4 inches. At supersonic Mach numbers up to 1.20 there appears to be impingement on the model of compression waves that are a reflection of the expansion waves that occurred over the forward portion of the model as the flow recovered to freestream conditions. This effect was seen in the data of references 2 and 4 for the expansion flow at the corners of cone cylinders and is discussed in reference 4. This will be discussed later in the section entitled Boundary-Reflected Disturbance Lengths.

As the test Mach number increased and approached the body design Mach number of 1.3 (design  $C_p = 0$ ), the pressure distribution became flatter ahead of the boundary-reflected nose shock impingement point, the location of which will be discussed later. There is a pressure increase near the base of the body at all Mach numbers below 1.20 that is associated with the flow over the model base and is perhaps also affected by the proximity of the sting flare and the bluntness of the sting-adapter (see figs. 1 and 2). However, the absence of flow field visualization data and pressure measurements in the model base and sting area prevents making any conclusions on the influence of the sting flare and the blunt sting-adapter. Experience has shown that it is good practice in transonic wind tunnel testing to design the model installation to minimize the effect of the model support hardware on the aft portion of the model whenever possible. In general terms this usually consists of having a sting-to-model base diameter ratio of about 0.5 with a constant sting diameter section approximately 5 model base diameters long followed by a total sting-flare half-angle of less than  $8^\circ$ . These criteria are considered to be reasonable to prevent pressurization of the aft portion of the model by the flow field of the support system and also of assuring that shocks created by the support system are well aft of the base region of the model. Based on the aforementioned "rule-of-thumb" criteria the sting support system of the present investigation would fail to meet the constant sting diameter length requirement. However there should be no effect on reflected-shock impingement points until the Mach number is large enough for the impingement point to approach the model base. More detailed information on the criteria pertinent to sting interference at the model base is contained in references 5 and 6.

In order to obtain pressure distributions with the closely spaced row of model orifices in other than the vertical plane, the model was rolled about its centerline at  $0^\circ$  angle of attack at Mach numbers from 1.00 to 1.25 (fig. 4). This data indicates that there was no significant effect of model roll

orientation on the pressure distributions even when the row of pressures was in the plane of the centerlines of two opposite test section slots ( $\phi_m = 22.5^\circ$ ). The apparent effects of body roll angle on the pressure distributions at some of the lower supersonic Mach numbers are attributable to small differences in Mach number setting at some of the roll angles. This effect of small differences in free stream Mach number is illustrated in figure 4(a) where at  $\phi_m = 0^\circ$  data was obtained at Mach numbers of 1.030 and 1.032. If the solid circles are compared to the open circles, a considerable difference in pressure distributions is evident. However if the pressures at  $\phi_m = 22.5^\circ$  which were obtained at a Mach number of 1.033 are compared to the solid symbols, it can be seen that they are nearly identical.

A graphical representation of the sensitivity of reflected-shock impingement location to small variations in Mach number at low supersonic Mach numbers is presented in figure 8 for the Mach number 1.05 data of figure 4(b) using greatly exaggerated scales. At this nominal Mach number setting, pressure distributions were obtained at  $22.5^\circ$  model roll angle increments between  $0^\circ$  and  $180^\circ$ . However, as roll angle was changed Mach number varied slightly within the accepted setting tolerance range of tunnel parameters. This allowed the selection of two orifices in the steep compression and expansion portions of the flowfield downstream of the impingement point to illustrate graphically the movement of the impingement point. As can be seen in figure 8 by the opposite nearly linear trends of pressures measured at the two locations, the variation in impingement point resulting from model roll angle (fig. 4(b)) is caused by the small variations in Mach number.

### **Effect of Plenum Suction at Mach Number 1.05**

The wind tunnel is calibrated to obtain a Mach number of 1.05 with and without the use of a test section plenum suction system. When this system is used, air is removed from the plenum by a compressor and there is a flow of test-section boundary-layer air through the slots into the plenum to replace air that is being exhausted to the atmosphere. These two methods of setting a Mach number of 1.05 were included in the test plan to determine if test section air removal through the slots affected the test section boundary-reflected-disturbance characteristics. Data was obtained at angles of attack of  $-9.3^\circ$ ,  $0^\circ$ , and  $10.0^\circ$  and is shown in figure 5. There was no discernable effect of plenum suction at  $0^\circ$  angle of attack on the pressure distribution and the small effects on the boundary-reflected-disturbance impingement point on the

body at angle of attack are once again attributable to the small differences in Mach number shown in the figure keys.

### **Pressure Coefficient Distribution at Angle of Attack**

Angle of attack effects on the body pressure distributions in the supersonic Mach number range are shown in figures 6 and 7 for the body oriented at  $\phi_m = 0^\circ$  and  $90^\circ$ . With the closely spaced row of pressure orifices on the top of the model (fig. 6) angle of attack affected the pressures as would be expected. That is, at negative angle of attack (orifice row on the windward side) the bow shock affecting the top row of pressures was stronger and therefore a steeper recovery occurred. When the closely-spaced row of pressure orifices was on the side of the model (fig. 7) angle of attack in effect put them in a cross flow. In this case the difference between the most forward pressure on the nose and the flatter pressure distribution on the mid-portion of the model at angle of attack was about the same as at  $0^\circ$  angle of attack. That is, the shape of the pressure distribution curves were the same at all 3 angles of attack; but the curves were displaced. Despite the fact that the tip of the nose moved off the test section centerline at angle of attack the impingement point for boundary-reflected disturbances stayed essentially the same as at  $0^\circ$  angle of attack (figs. 6 and 7) because the base of the model moved off the centerline in the opposite direction since the center of rotation for angle of attack was approximately at the midpoint of the model (fig. 2).

### **Boundary-Reflected Disturbance Lengths**

Most of the pressure distributions of figure 3 for supersonic speeds show the impingement of two major disturbances on the model. The upstream disturbance impingement point is believed to be caused by the reflection from the tunnel wall of expansion waves generated by the contour of the forebody. In reference 2 it was concluded from tunnel wall pressure measurements that expansion waves from the corner formed by the intersection of the conical nose with the cylindrical afterbody were reflected back to the model for models having a blockage ratio of 0.00098 or greater but not for a model having a blockage ratio of 0.000062. Since no tunnel wall pressures were recorded during the present investigation and the model blockage ratio was 0.000575 it is not possible to know if the expansion waves reached the tunnel walls. However, based on the pressure distributions it appears likely that the expansion waves were reflected back to the model as compression waves

(see also ref. 4). This expansion field is peculiar to model geometry downstream of the nose and its strength is related to model size. Therefore, since the subject of this paper concerns boundary reflected disturbance lengths for shocks generated by the model nose only those lengths are discussed and presented in figure 10.

The pressure distributions for supersonic speeds of figure 3 were examined to determine the  $x$  location of the start of the pressure rise from the boundary-reflected disturbance impingement of the nose shock. Determination of the location of this point below a Mach number of 1.03 was not possible but became evident as Mach number was increased above 1.03. The weak strength and Mach angle of the nose shock at the Mach numbers below 1.03 were not conducive to determination of an impingement point in the pressure recovery/expansion wave area occurring over the forward portion of the model. The reflected-disturbance impingement lengths for the nose-originated shocks are presented in figure 10 along with the relevant data from references 1 and 2. Reflected-disturbance length data from the current investigation ends at a Mach number of 1.08 due to the limited length of the model and the influence of the flow field around the model base and support system on the pressures sensed by the last 3 orifices. However, the nearly linear trends of this data and the trends obtained with longer bodies in references 1 and 2 indicate that, if required, some extrapolation for longer models at higher Mach numbers can be done with confidence.

The initial half angle of the model nose is about  $15^\circ$  with local half angle decreasing continuously with length due to the non-conical model shape such that at  $x = 11.375$  in. the chordal half angle ( $\tan^{-1} (d/2)/x$ ) is  $5.48^\circ$ . The trend of boundary-reflected disturbance length for this investigation shown in figure 10 is approximately aligned with the  $10^\circ$  half angle cone-cylinder data of figure 10 (model 1) indicating that the influence of the initial nose half angle on reflected-disturbance length is lessened considerably when the pointed nose is not conical. In utilizing the data of figure 10 for a planned model installation, it should be remembered that the wing and tail spans of a model, and model displacement from the centerline at angle of attack, need to be considered since the boundary-reflected disturbances may impinge on model components and still be downstream of the fuselage base at the centerline of the tunnel. The effect of model geometry can be estimated by making a scaled layout of the model in the test section and using the tip of the model nose and the impingement length of figure 10 to draw lines back to a point on the wall (this neglects

any wall boundary layer effect) at the appropriate shock or Mach angle to determine whether they pass close to or over any model components.

Bodies having noses that are not sharp will have quite different reflected-disturbance impingement lengths in that the nose shock will be stronger. It will stand ahead of (i.e. be detached from) the tip of the nose to higher Mach numbers, and will not bend over to the appropriate Mach angle until further from the centerline of the tunnel. In all cases the impingement lengths for non-pointed bodies will be shorter and will be greatly dependent on nose/forebody shape. Pre-test estimation of non-pointed-body reflection-free lengths for model sizing and test matrix planning purposes is more uncertain since most tunnels have very limited calibration data bases for this type of model geometry. Some early work on the estimation of detached shock-wave stand-off distances from the noses of bodies is reported in references 7 through 9. Unless it is clearly evident from estimates that there is no possibility of shock impingement within the planned test matrix, physical verification of the location of the reflected-disturbance impingement point by means of pressure data or flow field visualization is recommended.

## Concluding Remarks

An investigation has been conducted in the Langley 16-Foot Transonic Tunnel to determine boundary-reflected-disturbance lengths at low supersonic Mach numbers. A pressure instrumented body of revolution that had a nose designed to produce a bow shock and flow field similar to that about the nose of a supersonic transport configuration was used so that the lowest reflection-free supersonic Mach number could be determined. Test variables included Mach number (0.90 to 1.25), model angle of attack (nominally  $-10^\circ$ ,  $0^\circ$ , and  $10^\circ$ ), and model roll angle.

Results showed that the body, which had a blockage ratio of 0.000575, experienced interference associated with the reflection of the expansion field generated by the forward portion of the model at the lower supersonic Mach numbers. The model lengths that would be free of the bow-shock boundary-reflected disturbance were determined at Mach numbers from 1.03 to 1.08. When compared to bow-shock reflection lengths previously obtained on cone-cylinder bodies, it was found that the effect of the large nose initial-half-angle (approximately  $15^\circ$ ) on reflection-free length was lessened by the continuously decreasing local body half angle downstream of the nose. The variation of reflection-free length with Mach

number was fairly linear and showed essentially the same trend as cone-cylinder data. Model angle of attack did not affect the reflected-disturbance impingement point on the model since the center of rotation for angle of attack was approximately the midpoint of the model. When the model was rolled to direct the closely-spaced row of pressure orifices towards a test section slot no difference in pressure distributions was observed. Mach number 1.05 was set with and without the use of test section plenum suction and it was found that flow removal from the test section through the slots did not affect boundary conditions enough to be evident in reflection-free model lengths.

NASA Langley Research Center  
Hampton, VA 23681-2199  
October 1998

## References

1. Capone, Francis J.; Bangert, Linda S.; Asbury, Scott C.; Mills, Charles T.; and Bare, E. Ann: *The NASA Langley 16-Foot Transonic Tunnel. Historical Overview, Facility Description, Calibration, Flow Characteristics, and Test Capabilities*. NASA TP-3521, 1995.
2. Capone, Francis J.; and Coates, Edward M., Jr.: *Determination of Boundary-Reflected-Disturbance Lengths in the Langley 16-Foot Transonic Tunnel*. NASA TN D-4153, 1967.
3. Haglund, George T.; and Heinrich, Mark R.: *Shock Reflection Probe for Wind Tunnel Calibration and Investigation of Wall-Reflected Shocks*. AIAA-94-1935, 1994.
4. Estabrooks, Bruce B.: *Wall-Interference Effects on Axisymmetric Bodies in Transonic Wind Tunnels With Perforated Test Sections*. AEDC-TR-59-12, ASTIA Doc. No: AD-216698, U.S. Air Force, June 1959.
5. Cahn, Maurice S.: *An Experimental Investigation of Sting-Support Effects on Drag and a Comparison with Jet Effects*. NACA Rep. 1353, 1958.
6. Kennedy, T. L.: *An Evaluation of Wind Tunnel Test Techniques for Aircraft Nozzle Afterbody Testing at Transonic Mach Numbers*. AEDC-TR-80-8, U.S. Air Force, 1980.
7. Laitone, Edmund V.; and Pardee, Otway O'M.: *Location of Detached Shock Wave in Front of a Body Moving at Supersonic Speeds*. NACA RM A7B10, 1947.
8. Moeckel, W. E.: *Approximate Method for Predicting Form and Location of Detached Shock Waves Ahead of Plane or Axially Symmetric Bodies*. NACA TN 1921, 1949.
9. Heberle, Juergen W.; Wood, George P.; and Gooderum, Paul B.: *Data on Shape and Location of Detached Shock Waves on Cones and Spheres*. NACA TN 2000, 1950.

Table 1. Test Section Wall Divergence Angles Set for the Data Presented

M	$\delta$ , deg
0.90	4.9
0.92	6.2
0.94	8.0
0.96	10.3
0.98	13.2
1.00	14.2
1.02	9.6
1.03	8.6
1.04	7.3
1.05	6.0
1.06	5.0
1.08	4.0
1.10	1.0
1.15	17.8 or 18.7
1.20	7.6 or 8.7
1.25	14.0 or 15.5

Table 2. Shock Reflection Body Pressure Orifice Locations

x, in.	$\phi$ , deg			
	0	90	180	270
4.0	.			
4.5	.			
5.0	.			
5.5	.			
6.0	.			
6.5	.			
7.0	.			
8.5	.			
8.0	.			
8.5	.			
9.0	.			
9.5	.			
10.0	.	.	.	.
10.5	.			
11.0	.			
11.5	.			
12.0	.			
12.5	.			
13.0	.			
13.5	.			
14.0	.			
14.5	.			
15.0	.			
15.5	.			
16.0	.			
16.5	.			
17.0	.			
17.5	.			
18.0	.			
18.5	.			
19.0	.			
19.5	.			
20.0	.	.	.	.
20.5	.			
21.0	.			
21.5	.			
22.0	.			
22.5	.			
23.0	.			
23.5	.			
24.0	.			
24.5	.			
25.0	.			

x, in.	$\phi$ , deg			
	0	90	180	270
25.5	.			
26.0	.			
26.5	.			
27.0	.			
27.5	.			
28.0	.			
28.5	.			
29.0	.			
29.5	.			
30.0	.	.	.	.
31.0	.			
32.0	.			
33.0	.			
34.0	.			
35.0	.			
36.0	.			
37.0	.			
38.0	.			
39.0	.			
40.0	.			
41.0	.			
42.0	.			
43.0	.			
44.0	.			
45.0	.	.	.	.
46.0	.			
47.0	.			
48.0	.			
49.0	.			
50.0	.			
51.0	.			
52.0	.			
53.0	.			
54.0	.			
55.0	.			
56.0	.			
57.0	.			
58.0	.			
59.0	.			
60.0	.	.	.	.
61.0	.			
62.0	.			
63.0	.			



L-93-13127

(a) Model and arc sector support system.

Figure 1. Photographs showing the body of revolution, model support system and the test section of the 16-Foot Transonic Tunnel.

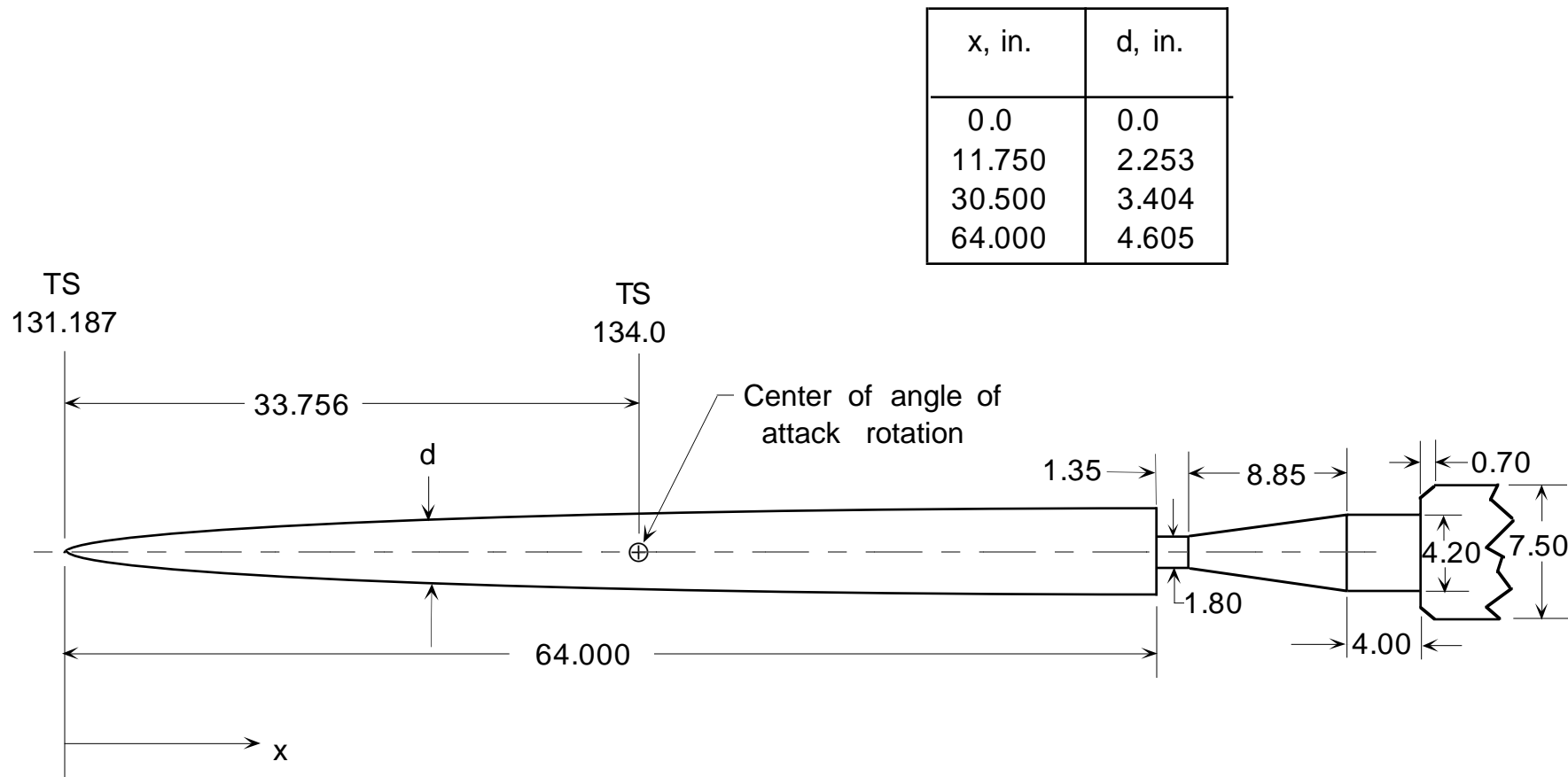
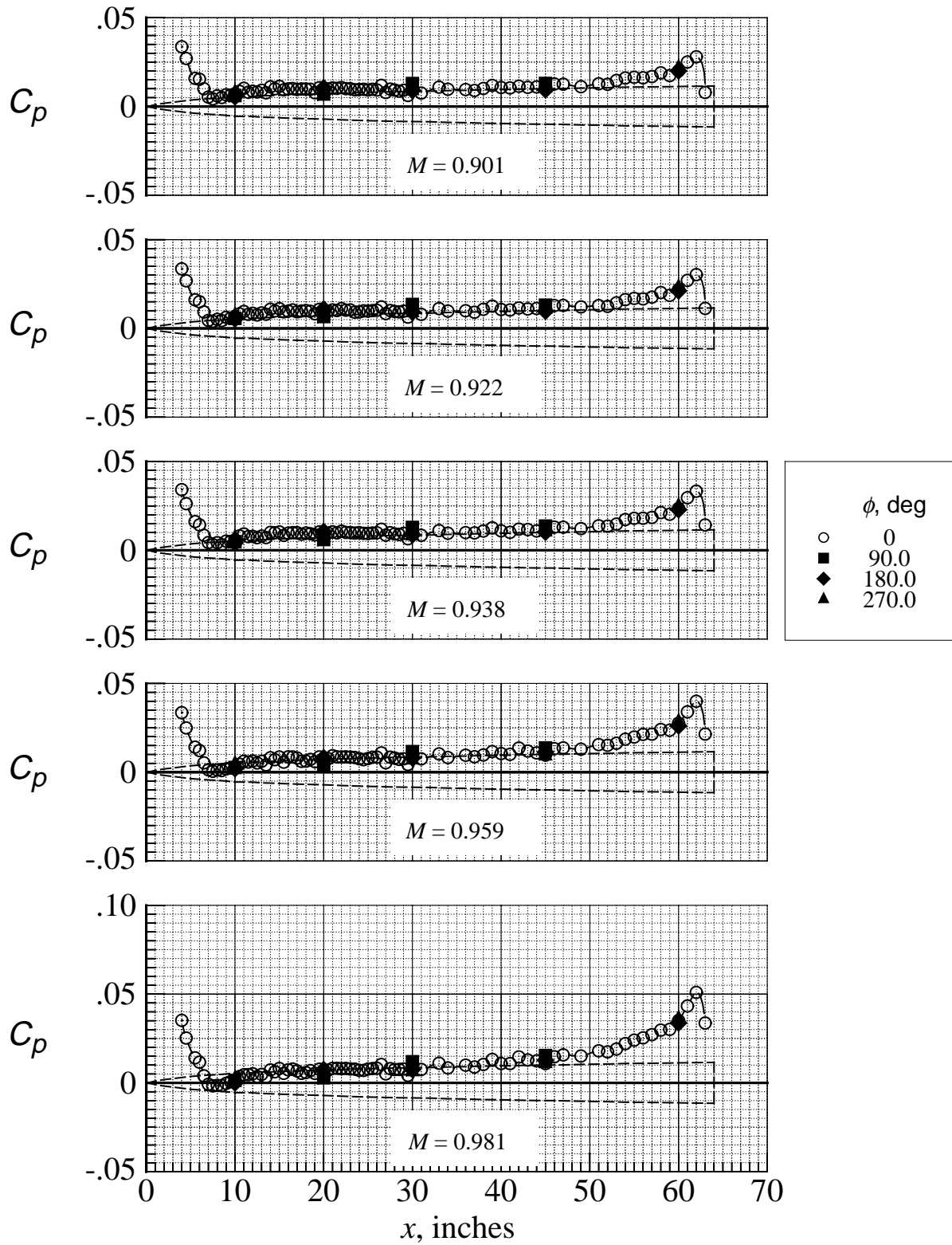
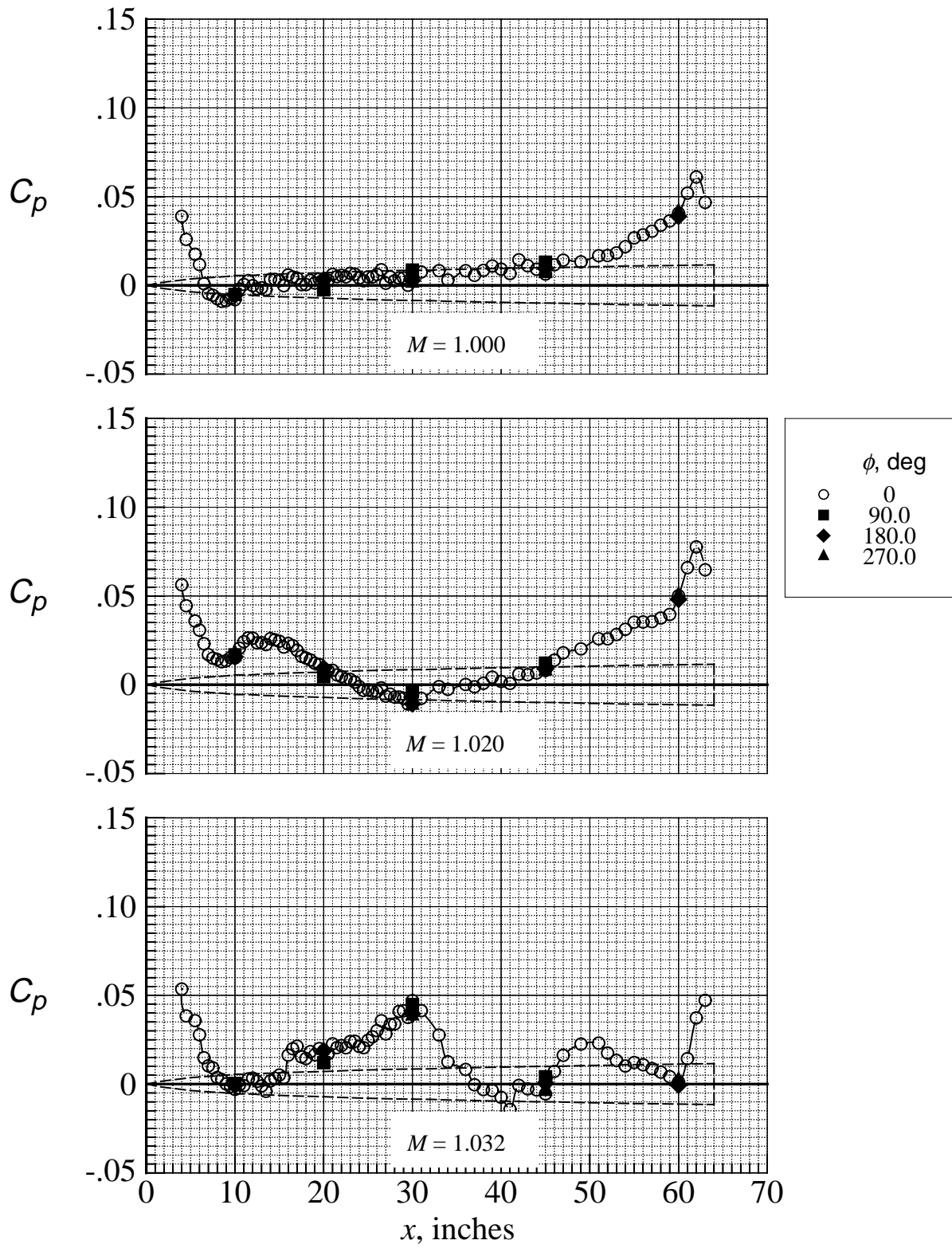


Figure 2. Sketch of model showing its longitudinal location in the tunnel test section. Dimensions are in inches except for tunnel stations (TS) which are in feet.



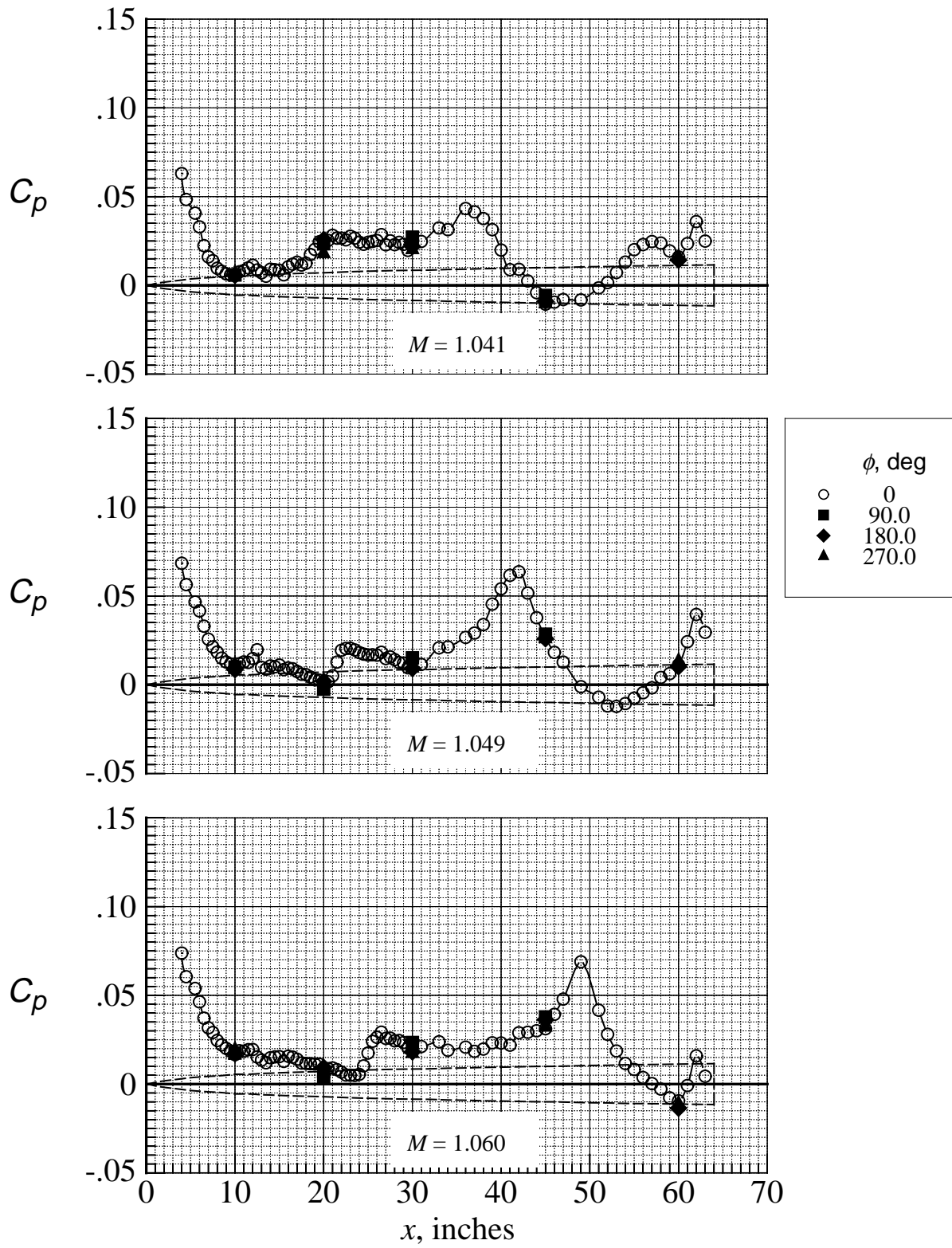
(a)  $M = 0.90$  to  $0.98$ .

Figure 3. Pressure distributions on the body at subsonic and supersonic Mach numbers for  $\alpha = 0^\circ$  and  $\phi_m = 0^\circ$ .



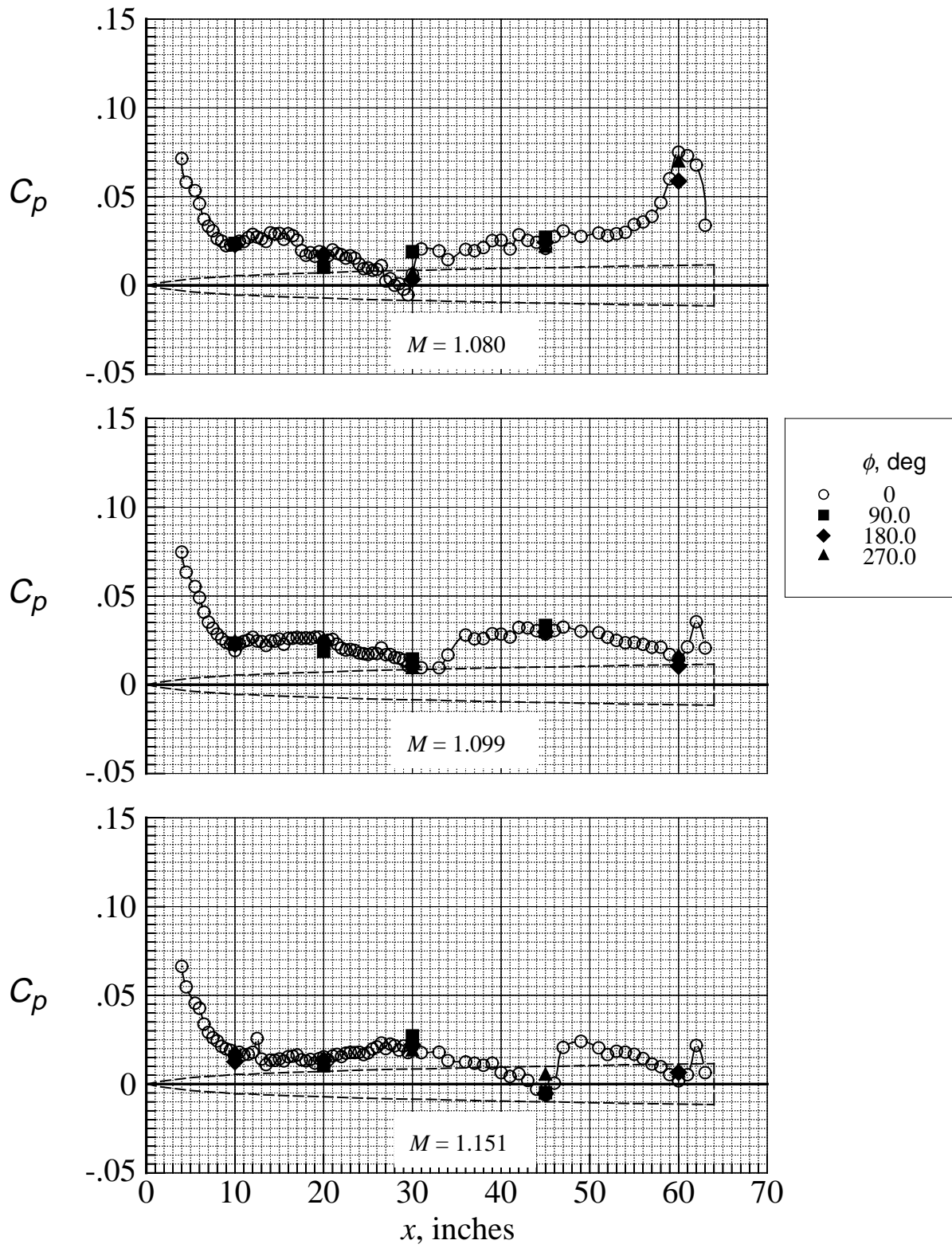
(b)  $M = 1.00$  to 1.03.

Figure 3. Continued.



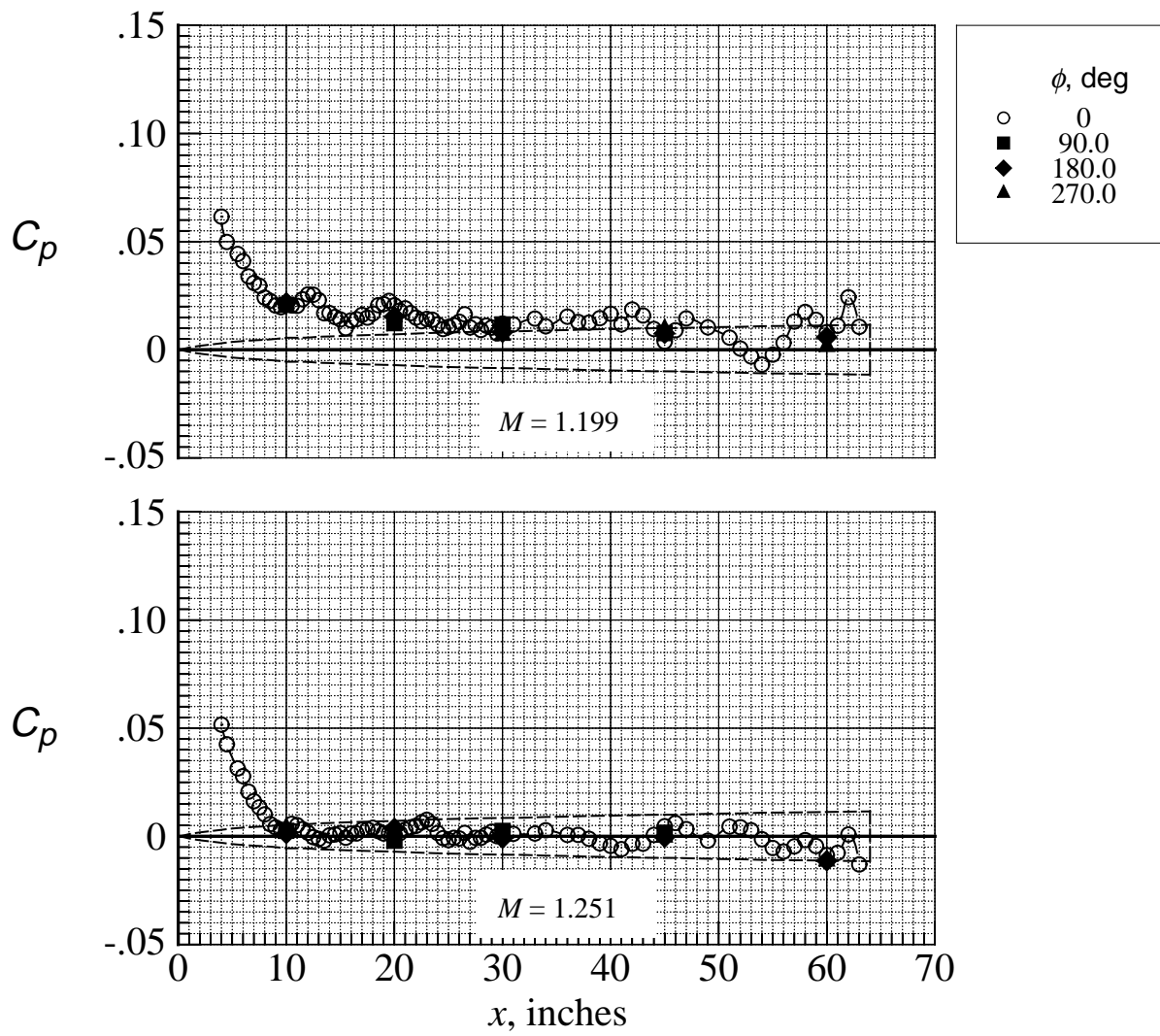
(c)  $M = 1.04$  to 1.06.

Figure 3. Continued.



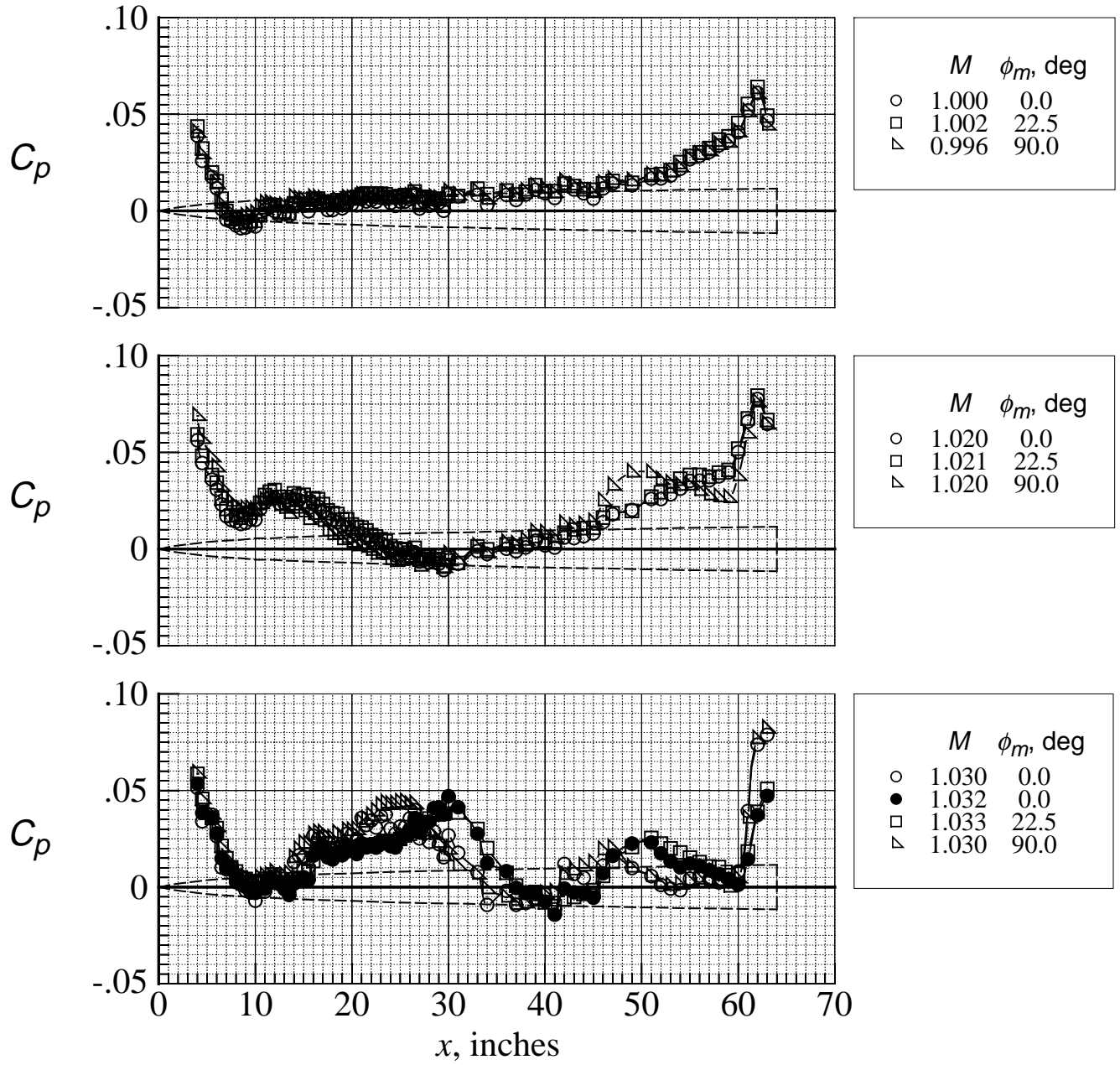
(d)  $M = 1.08$  to 1.15.

Figure 3. Continued.



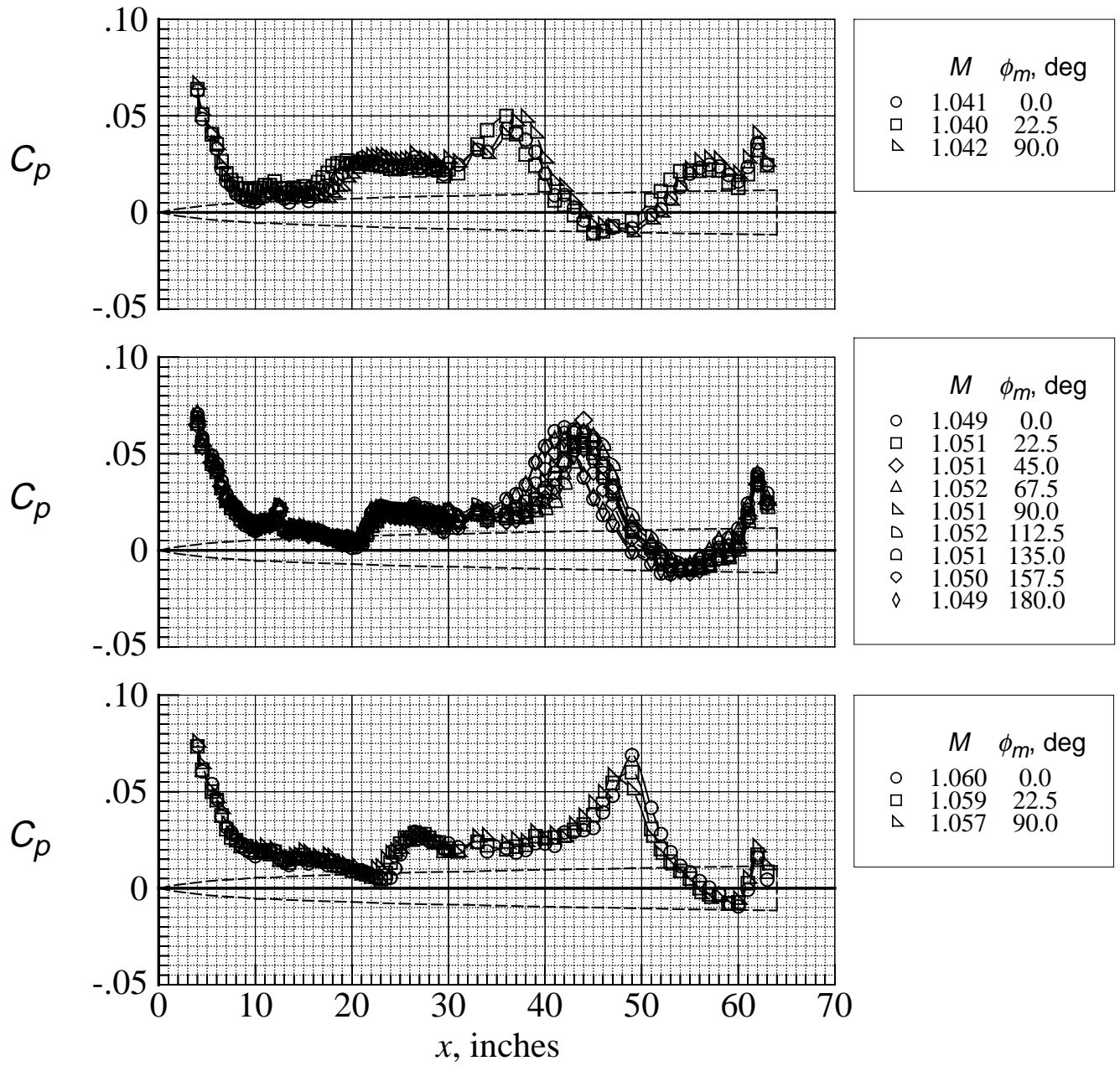
(e)  $M = 1.20$  and  $1.25$ .

Figure 3. Concluded.



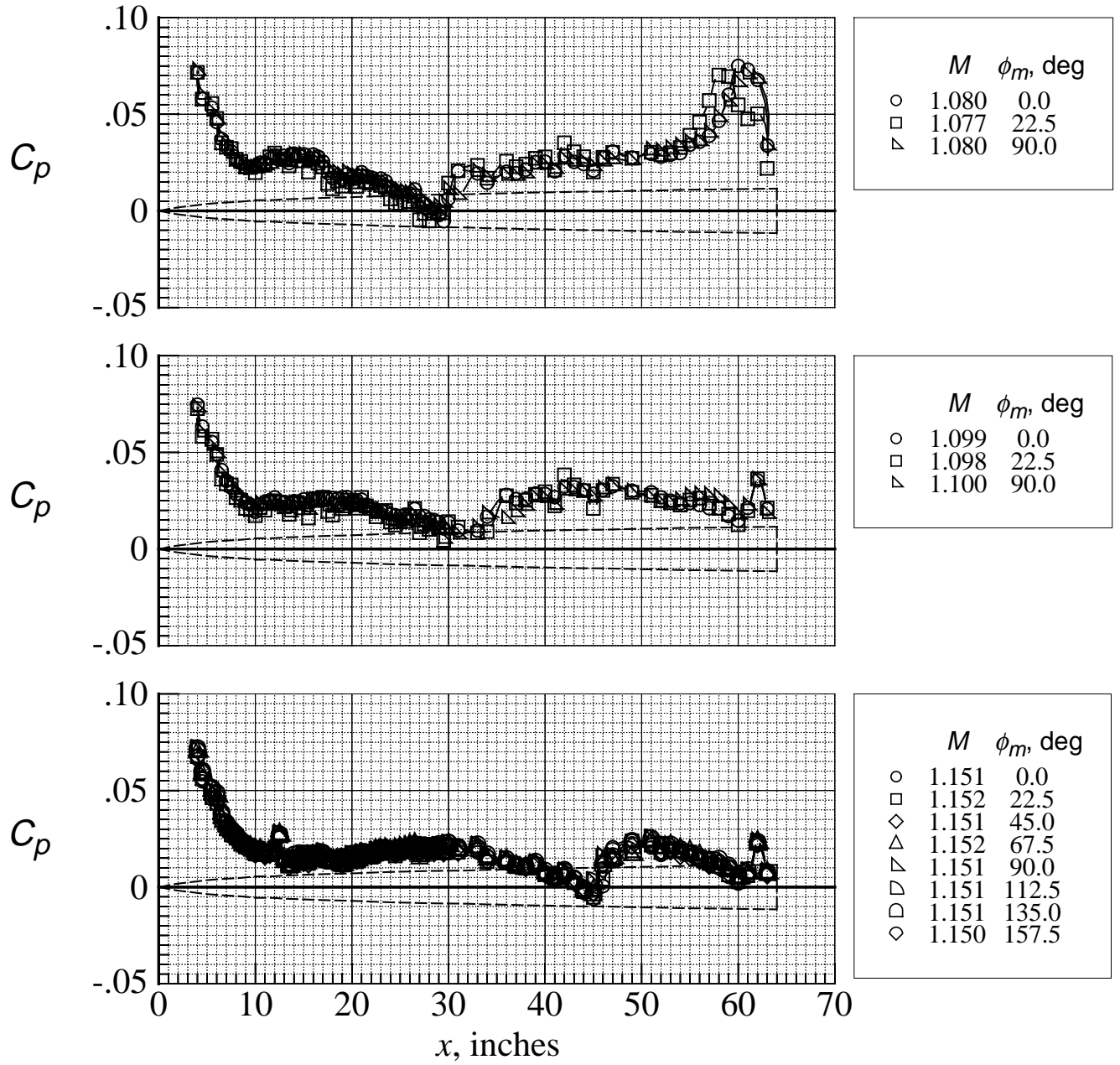
(a)  $M = 1.00$  to  $1.03$ .

Figure 4. Effect of model roll angle on pressure distributions measured by closely spaced longitudinal row of orifices,  $\alpha = 0^\circ$ .



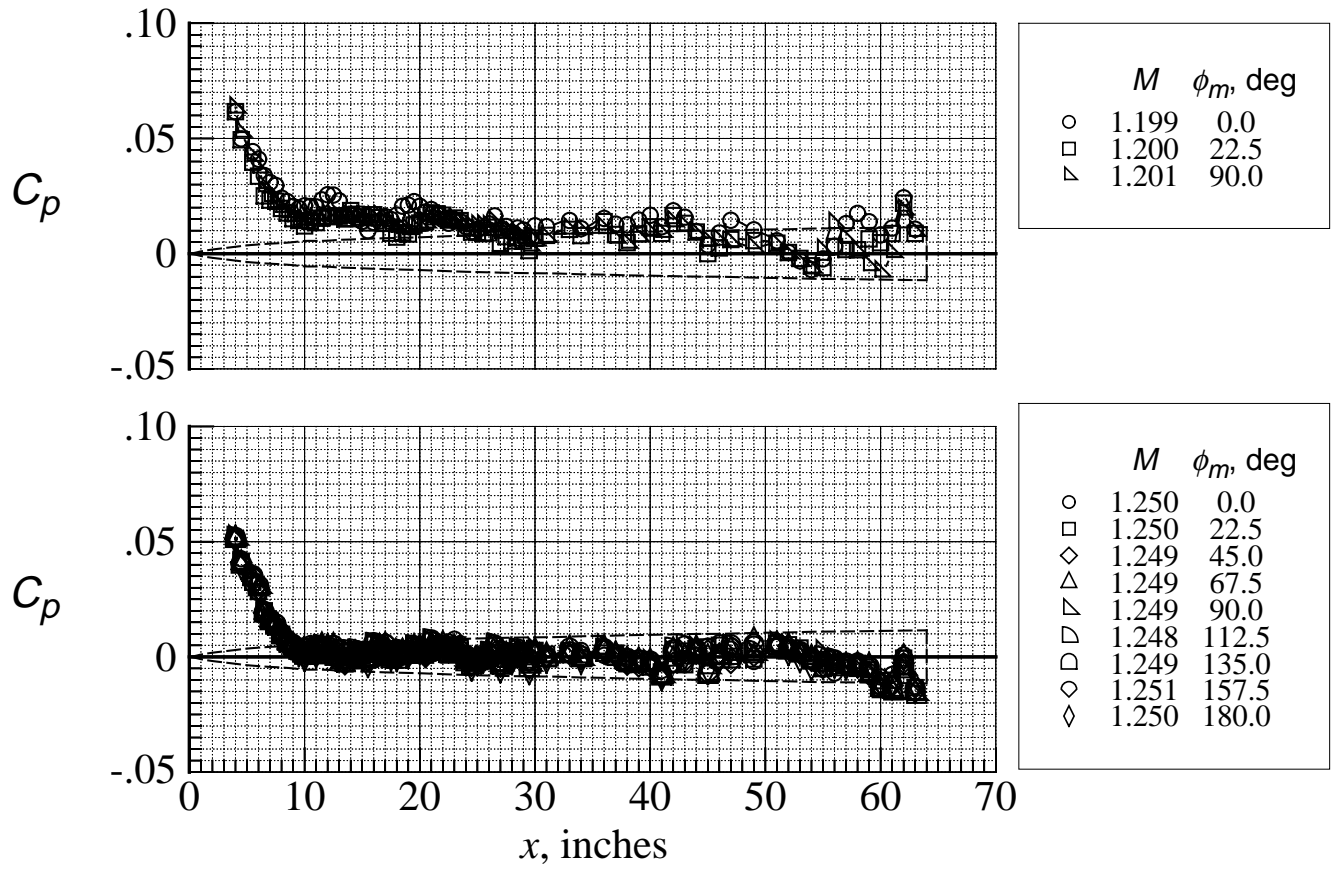
(b)  $M = 1.04$  to  $1.06$ .

Figure 4. Continued.



(c)  $M = 1.08$  to  $1.15$ .

Figure 4. Continued.



(d)  $M = 1.20$  and  $1.25$ .

Figure 4. Concluded.

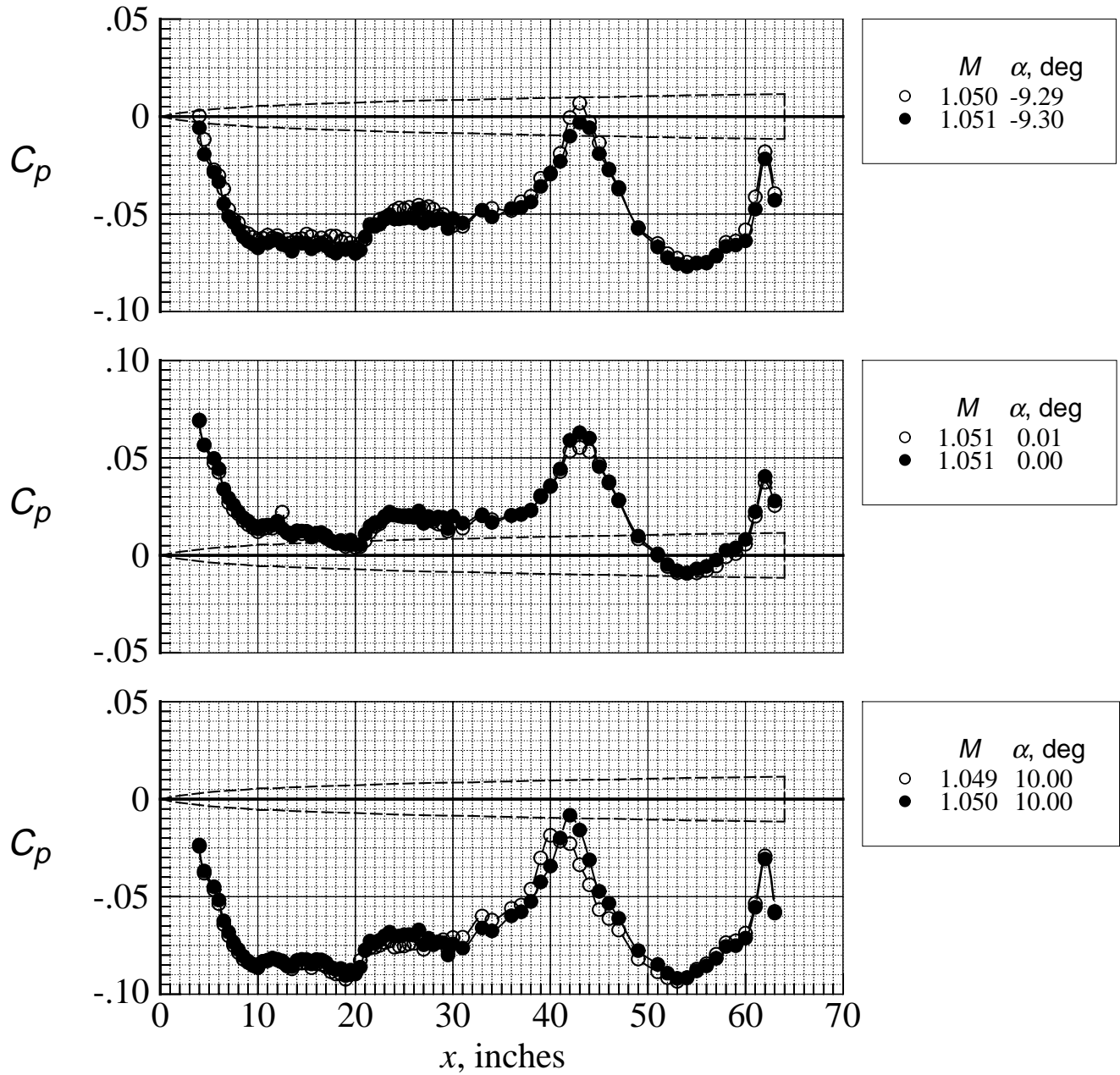
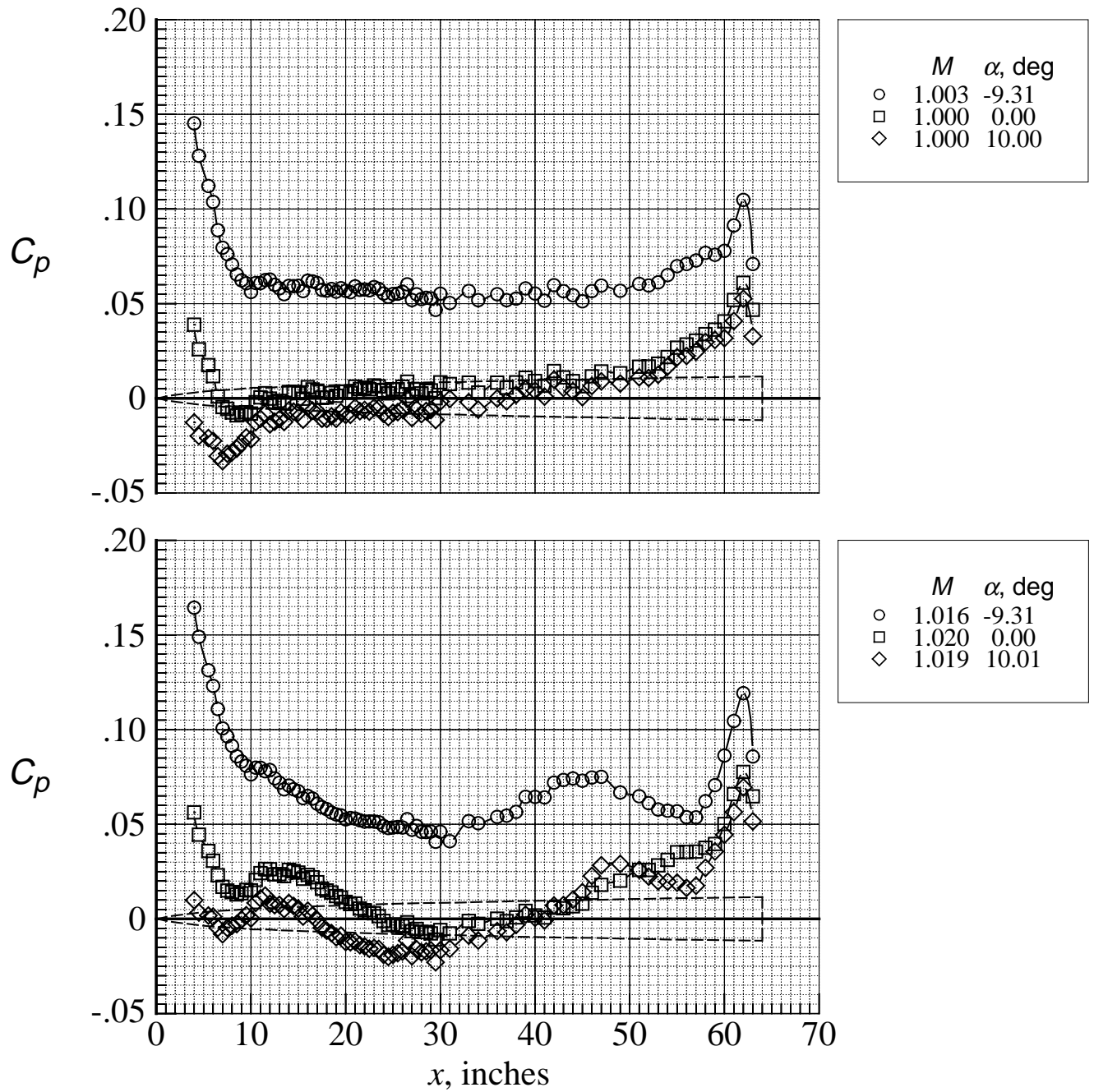
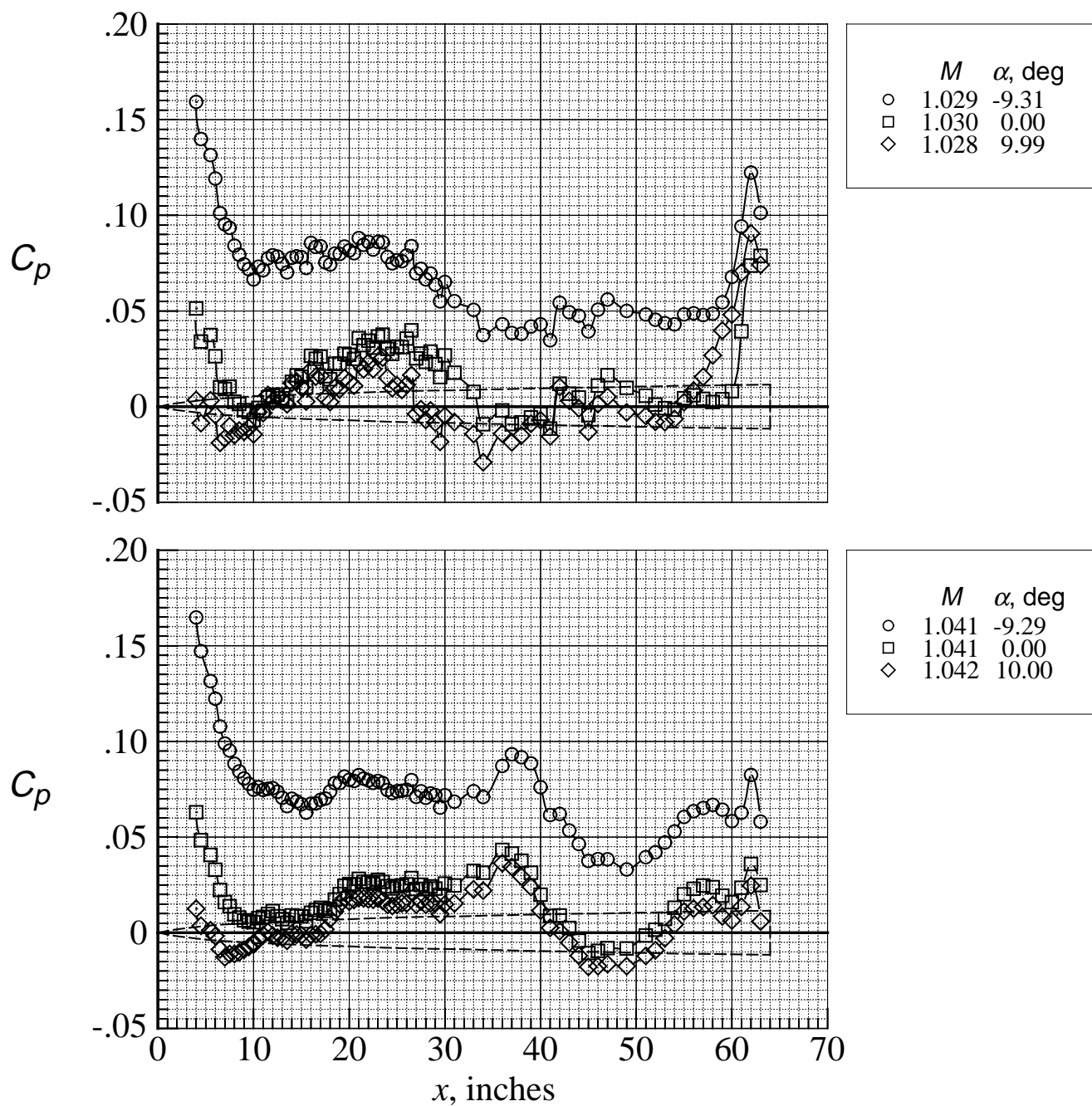


Figure 5. Pressure distributions on the body at a Mach number of 1.05 with test section plenum suction on and off,  $\phi_m = 90^\circ$ . (Open symbols indicate that test section plenum suction is being applied and solid symbols indicate plenum suction is off.)



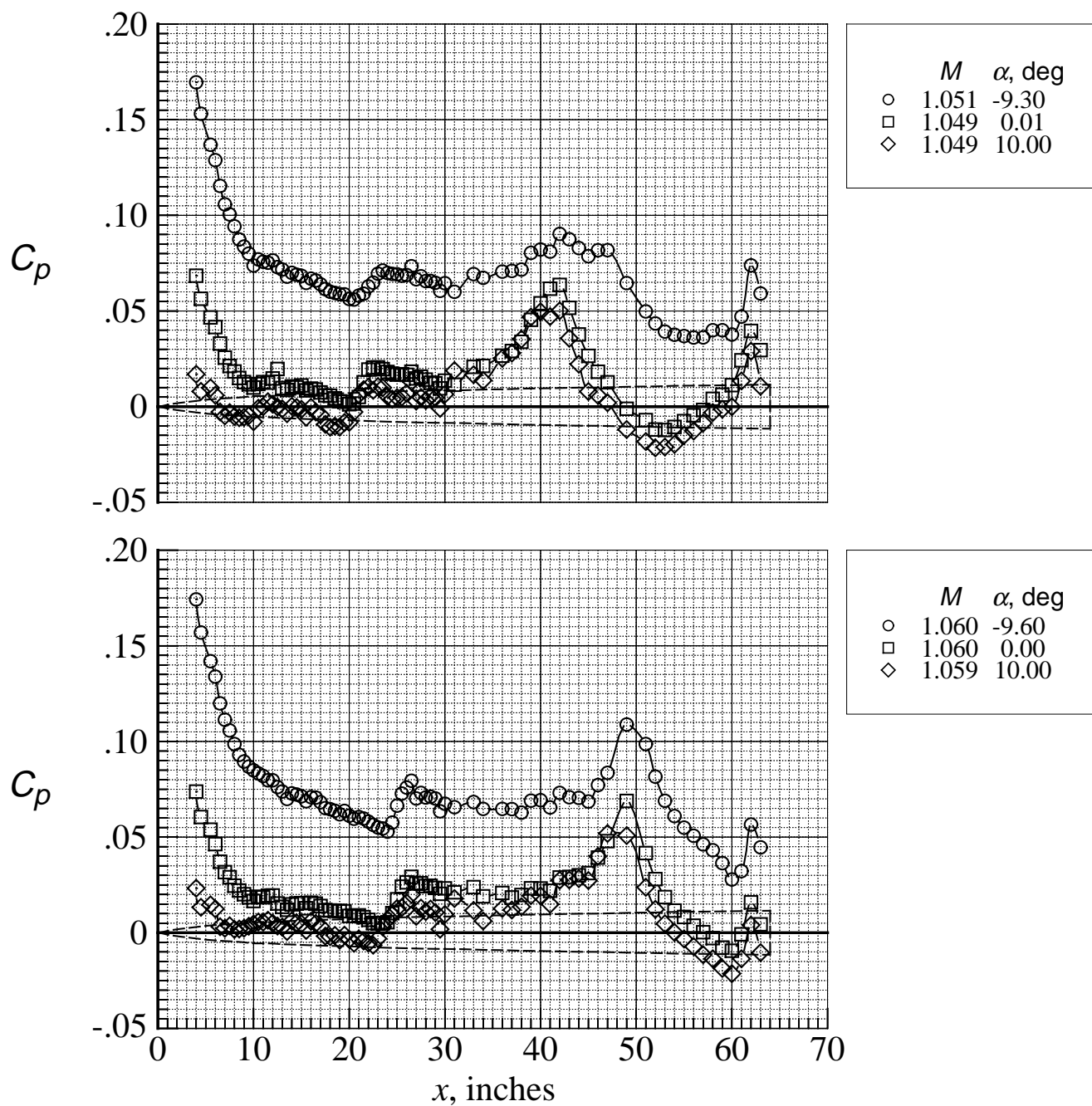
(a)  $M = 1.00$  and  $1.02$ .

Figure 6. Effect of angle of attack on body pressure distributions measured with the closely spaced longitudinal row of orifices on top of the model,  $\phi_m = 0^\circ$ .



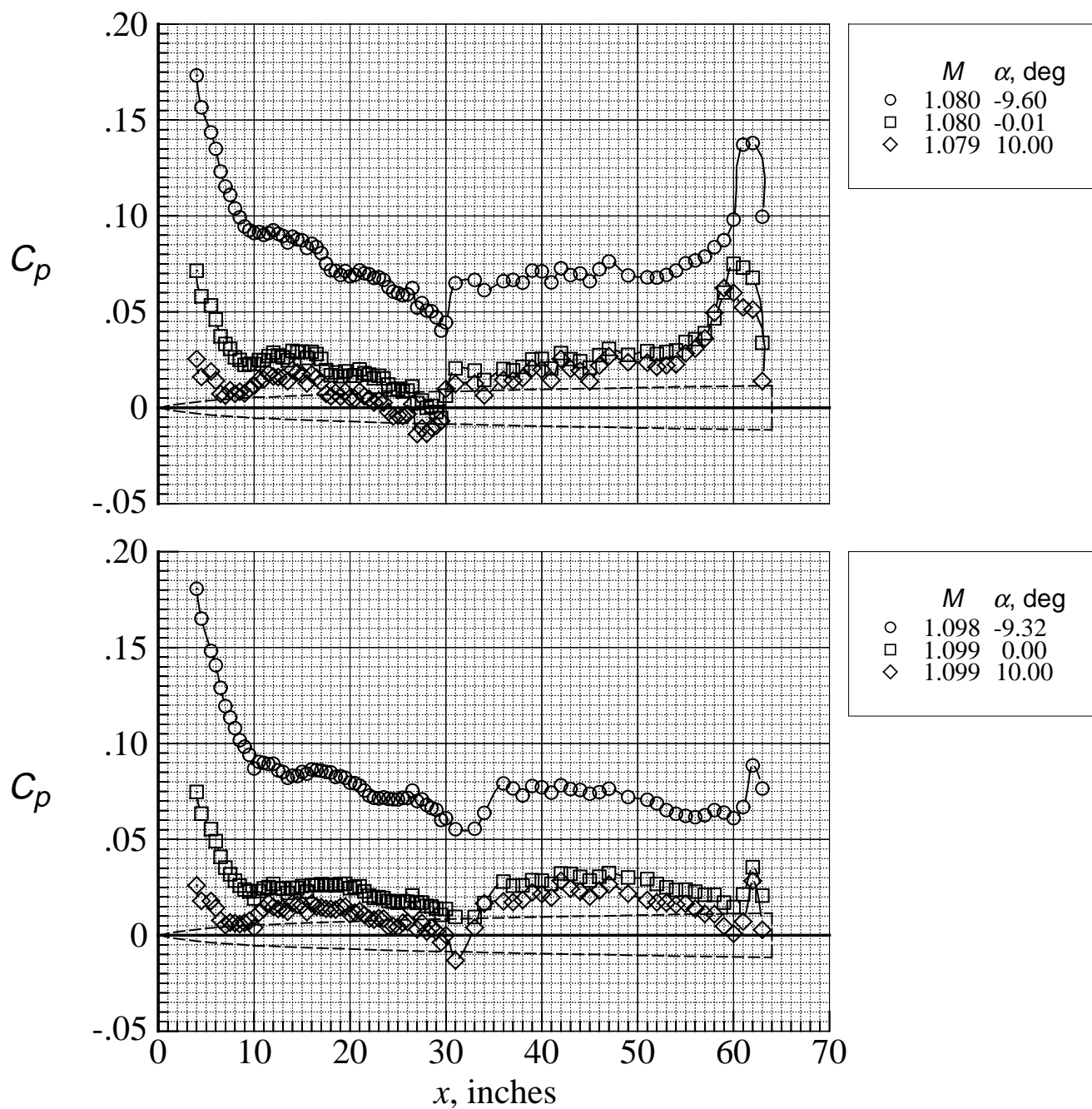
(b)  $M = 1.03$  and  $1.04$ .

Figure 6. Continued.



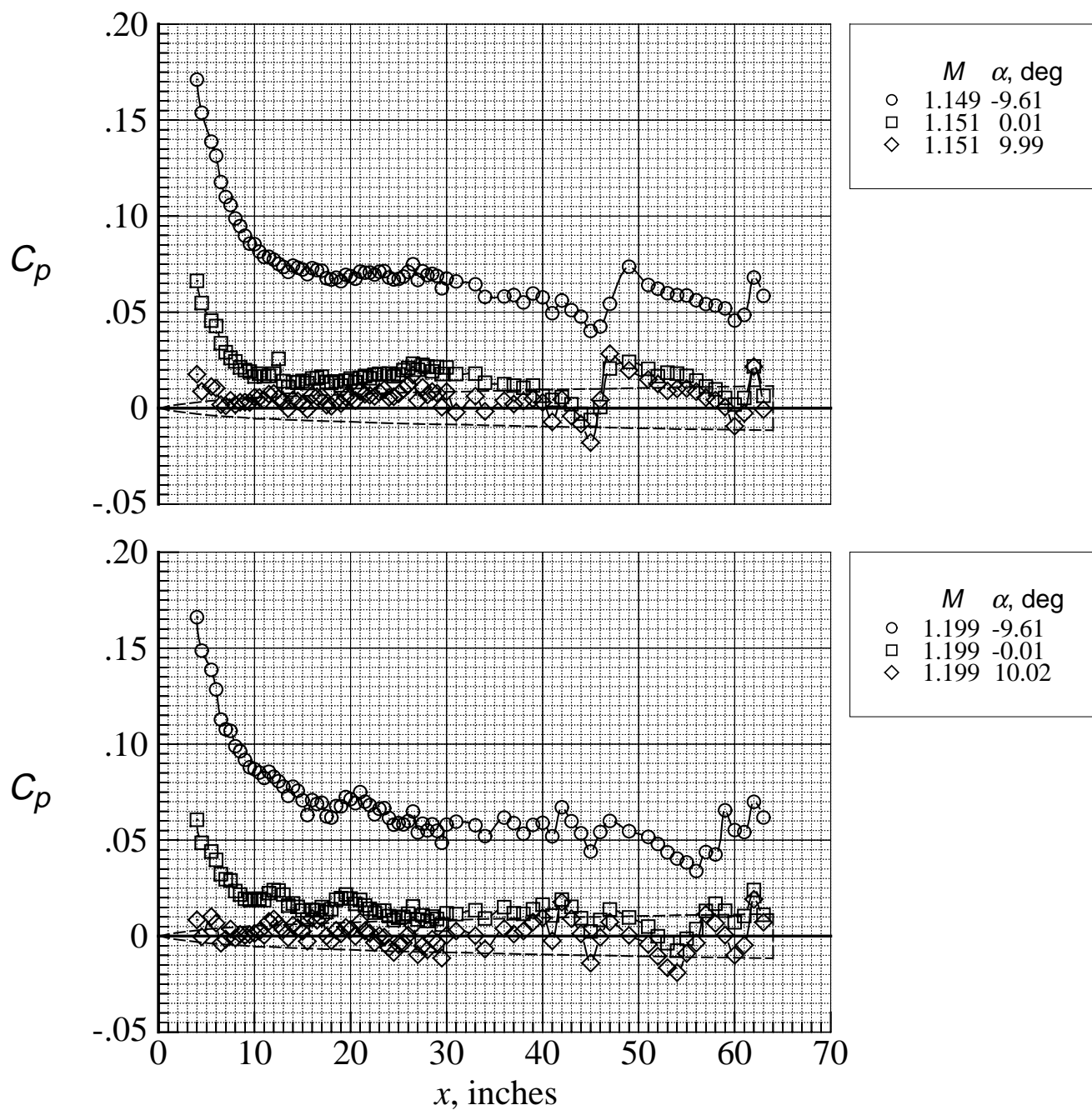
(c)  $M = 1.05$  and  $1.06$ .

Figure 6. Continued.



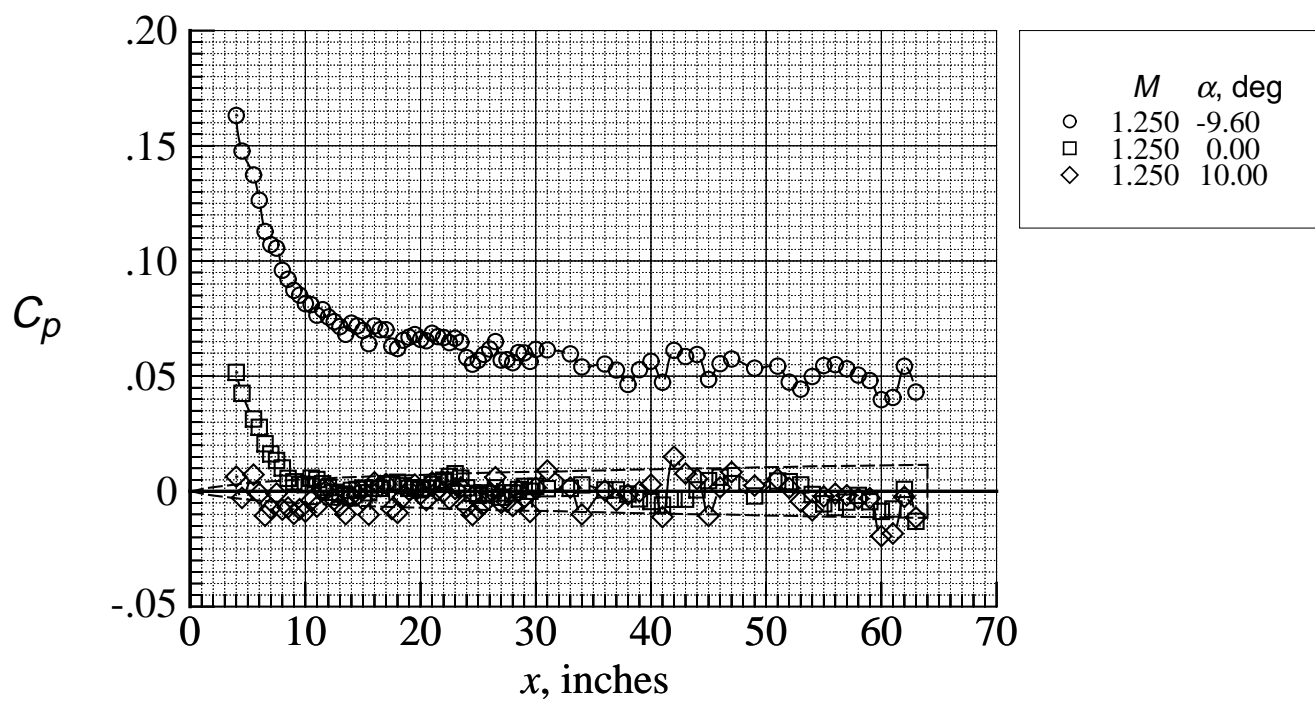
(d)  $M = 1.08$  and 1.10.

Figure 6. Continued.



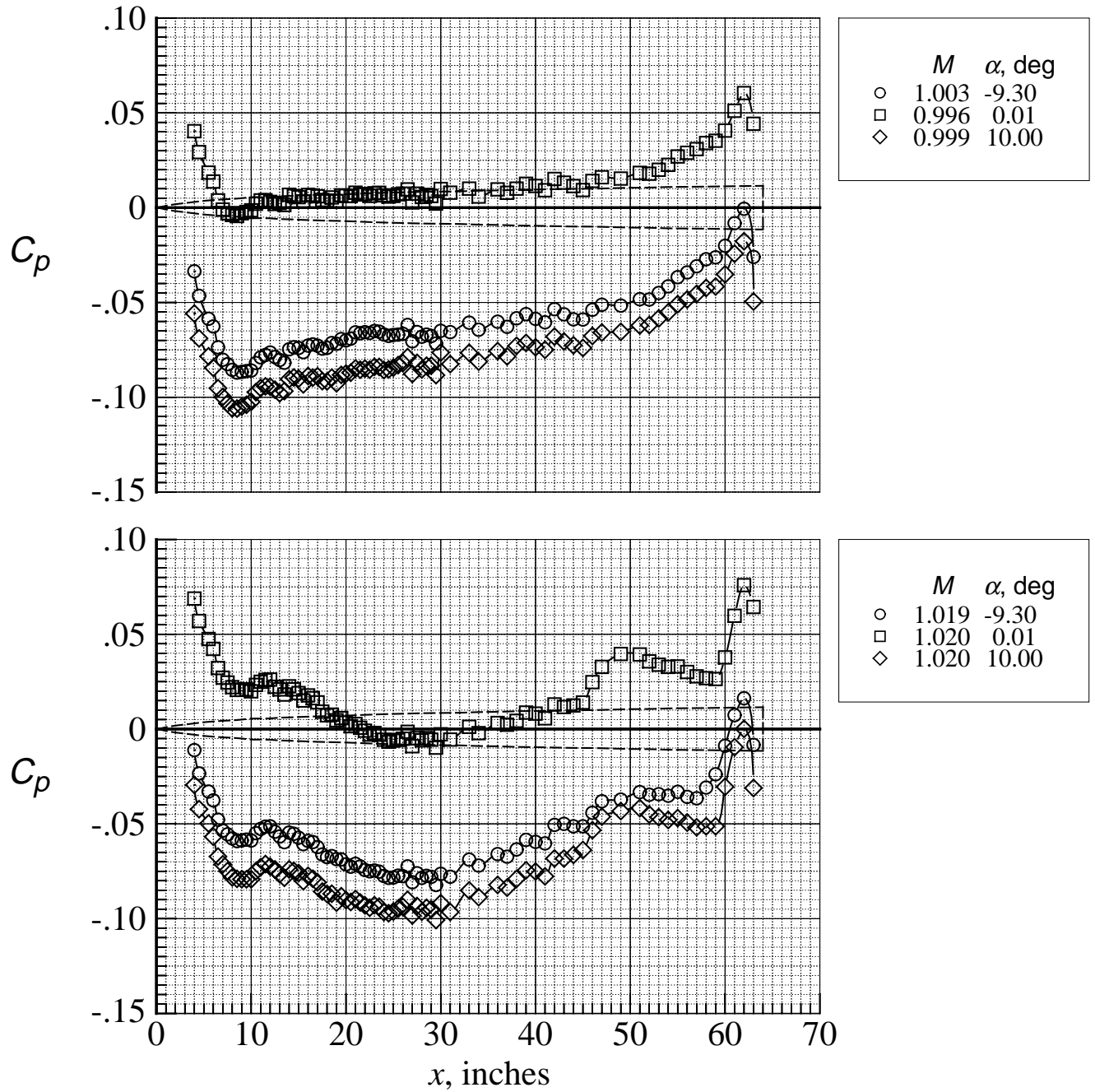
(e)  $M = 1.15$  and 1.20.

Figure 6. Continued.



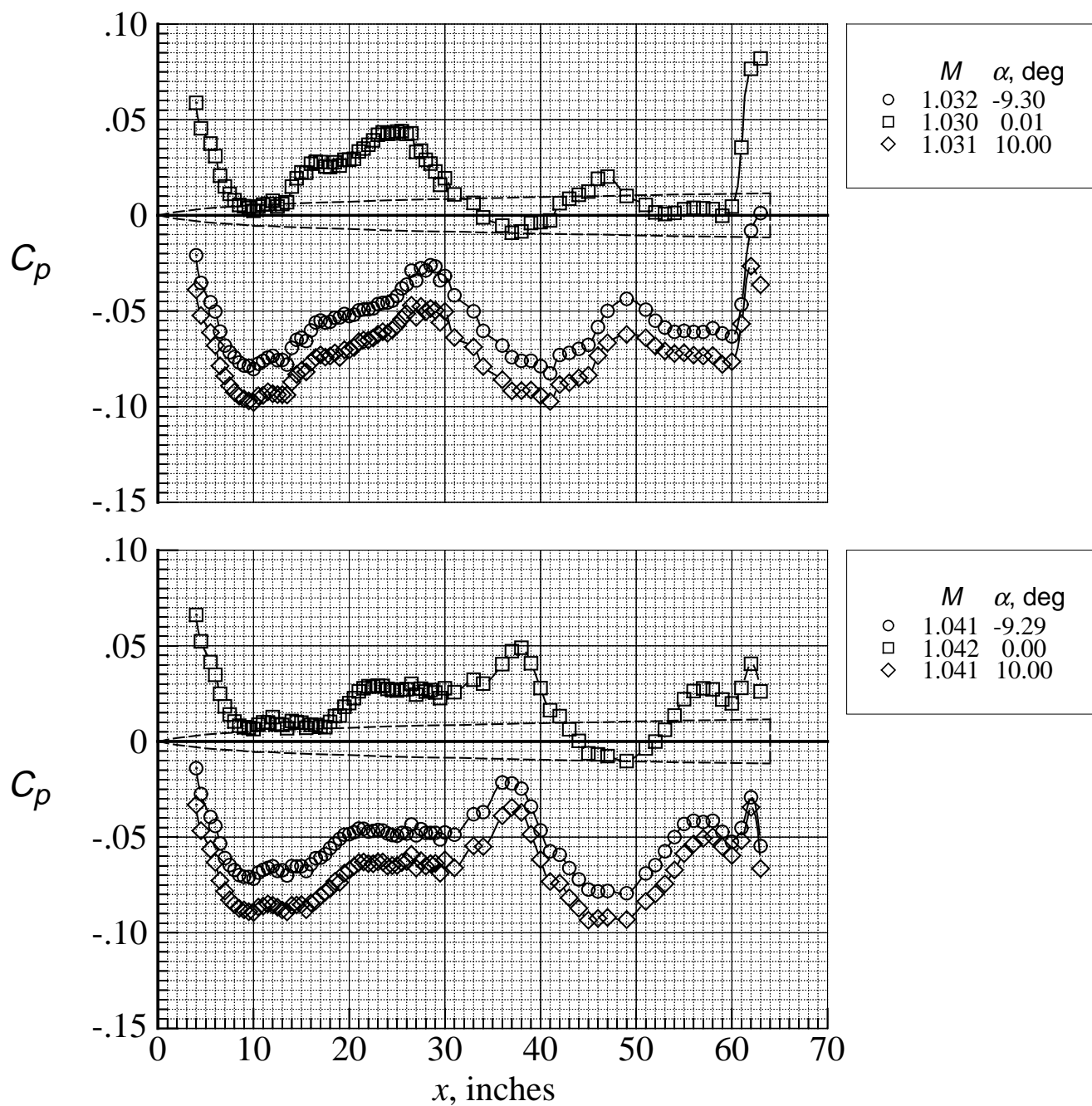
(f)  $M = 1.25$ .

Figure 6. Concluded.



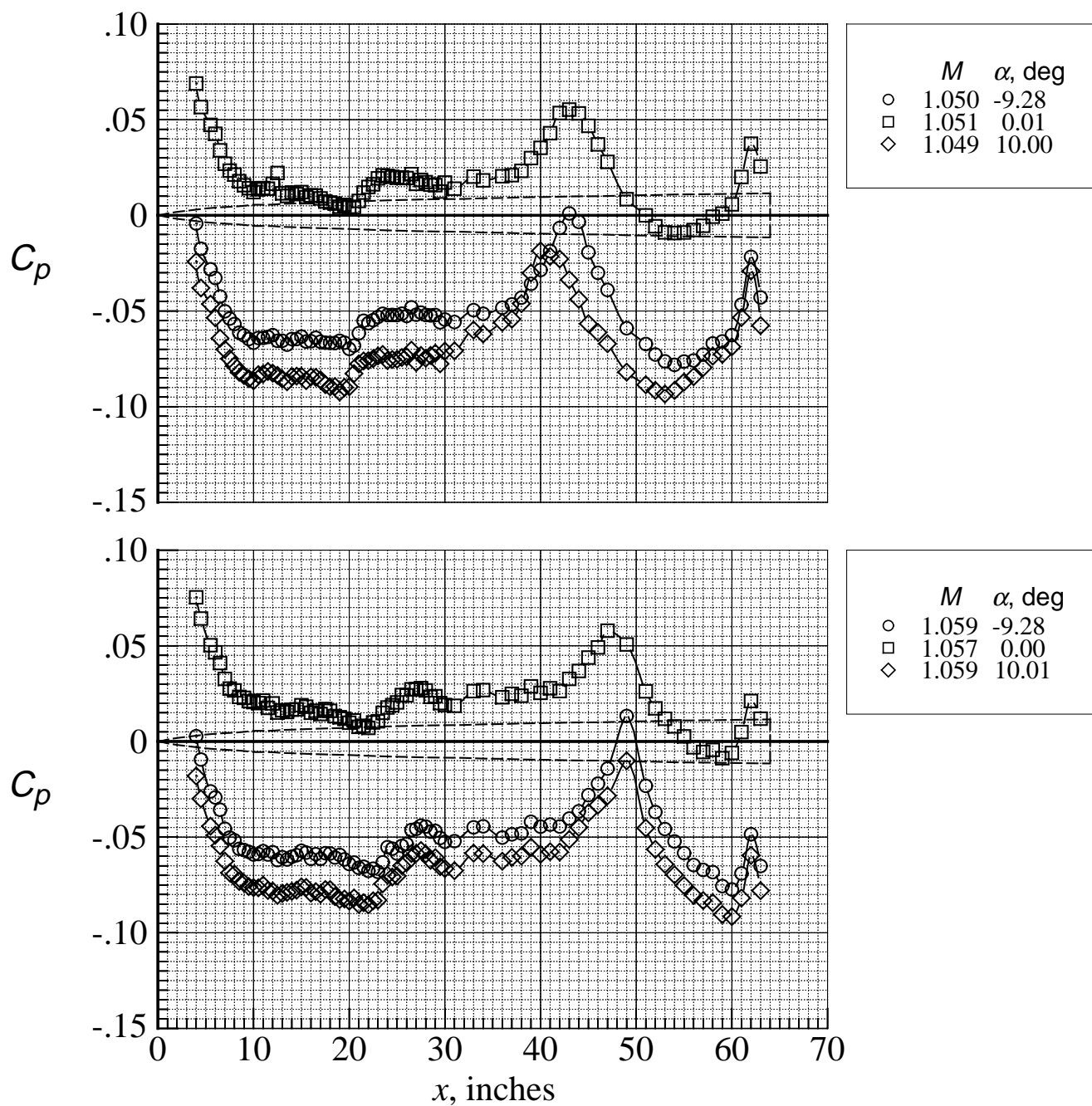
(a)  $M = 1.00$  and  $1.02$ .

Figure 7. Effect of angle of attack on body pressure distributions measured with the closely spaced longitudinal row of orifices on the side of the model,  $\phi_m = 90^\circ$ .



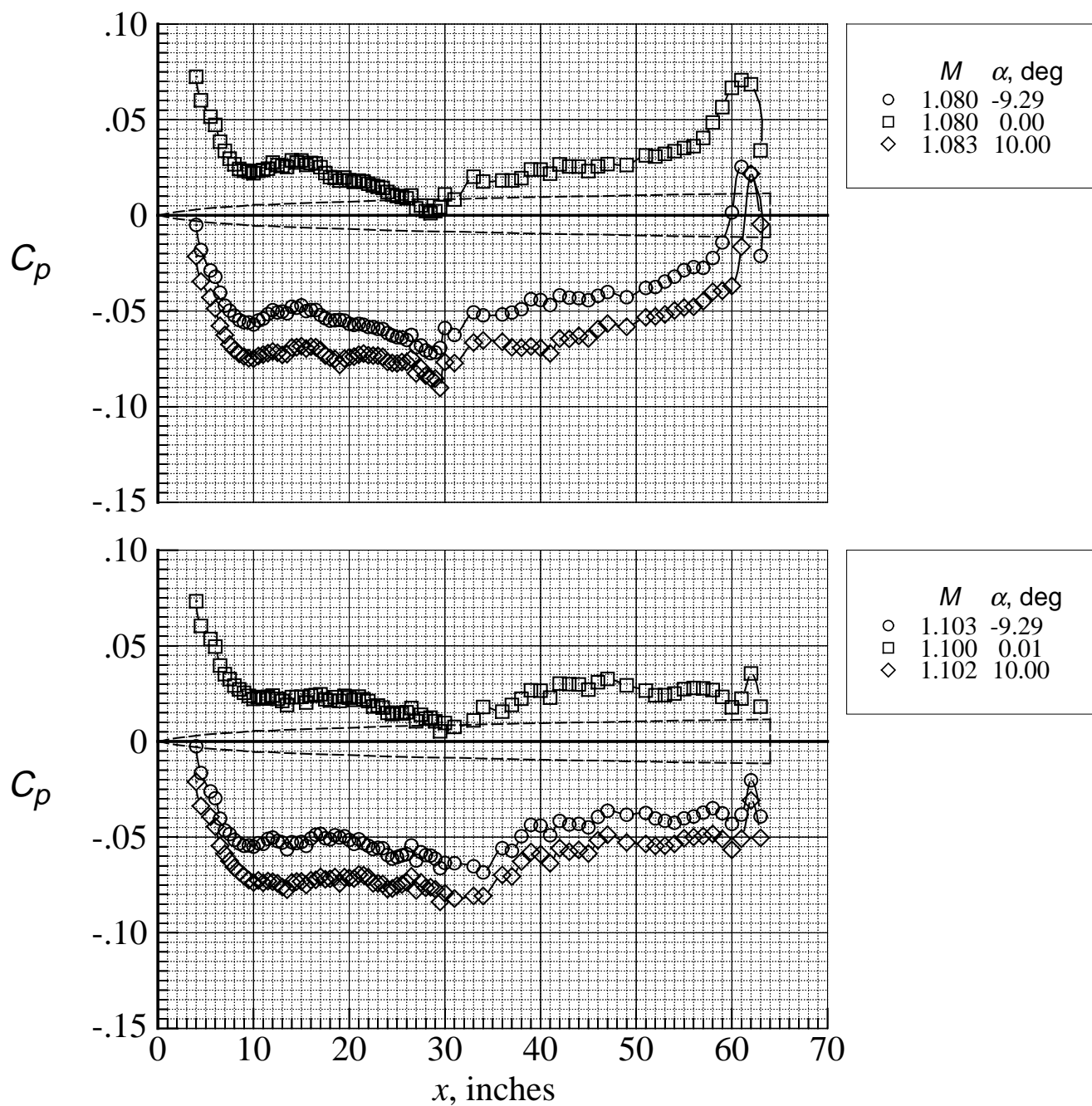
(b)  $M = 1.03$  and 1.04.

Figure 7. Continued.



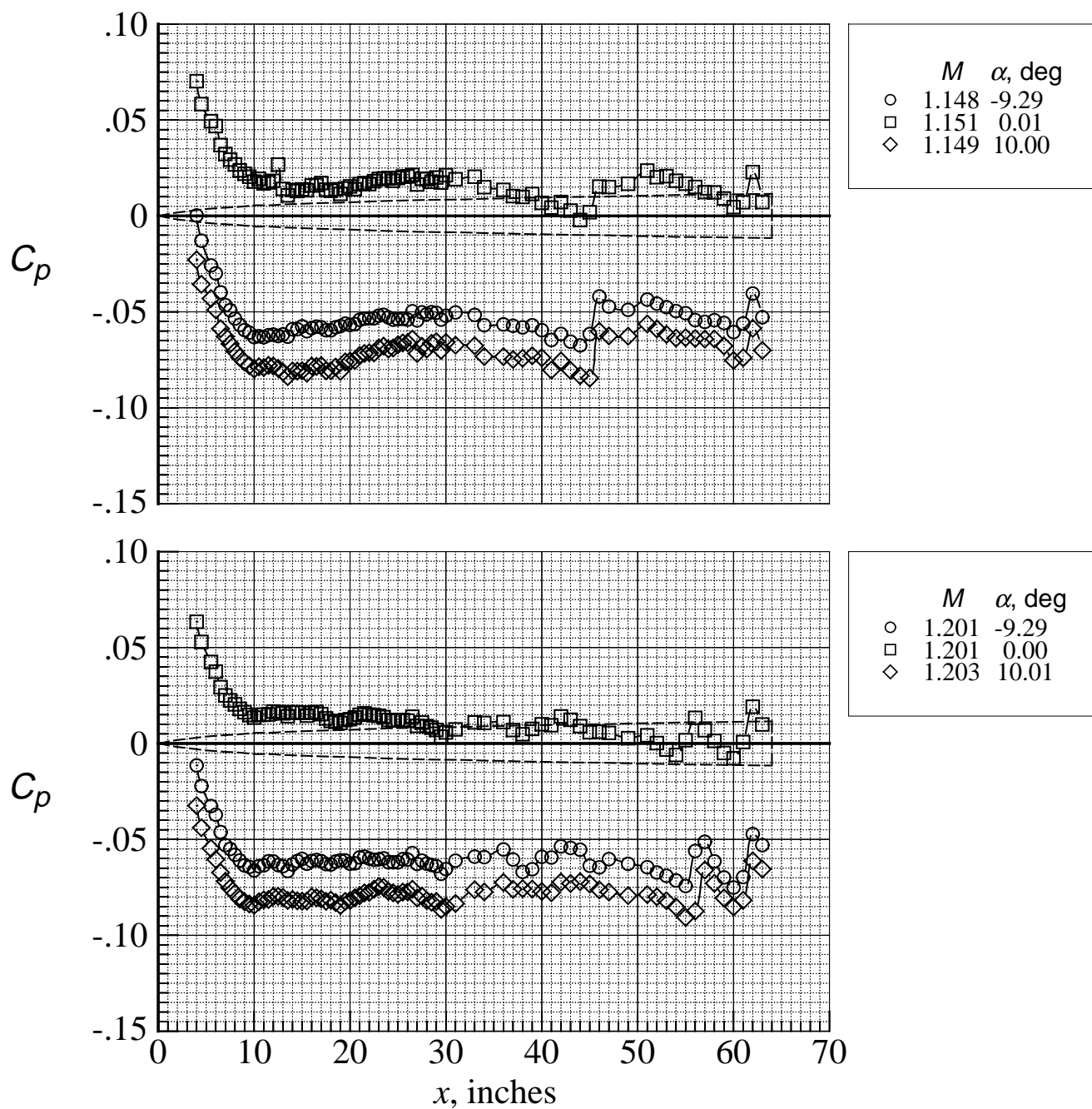
(c)  $M = 1.05$  and  $1.06$ .

Figure 7. Continued.



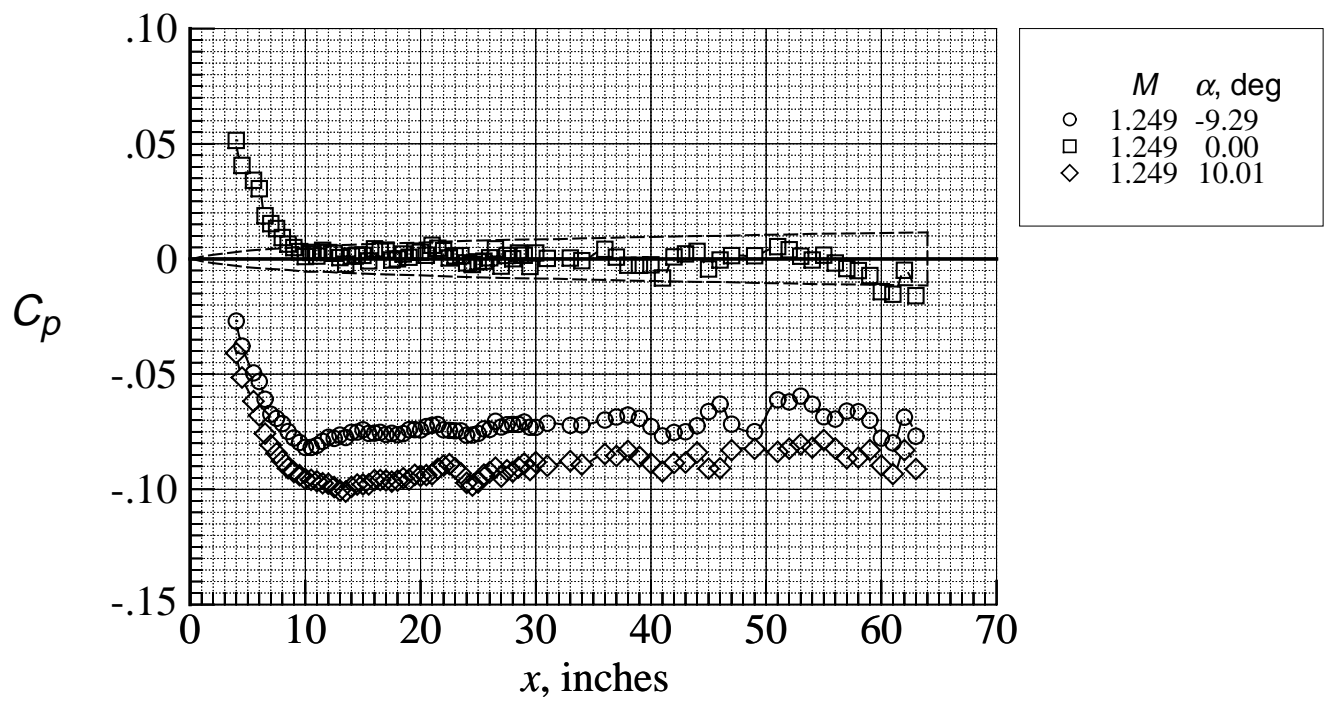
(d)  $M = 1.08$  and 1.10.

Figure 7. Continued.



(e)  $M = 1.15$  and 1.20.

Figure 7. Continued.



(f)  $M = 1.25$ .

Figure 7. Concluded.

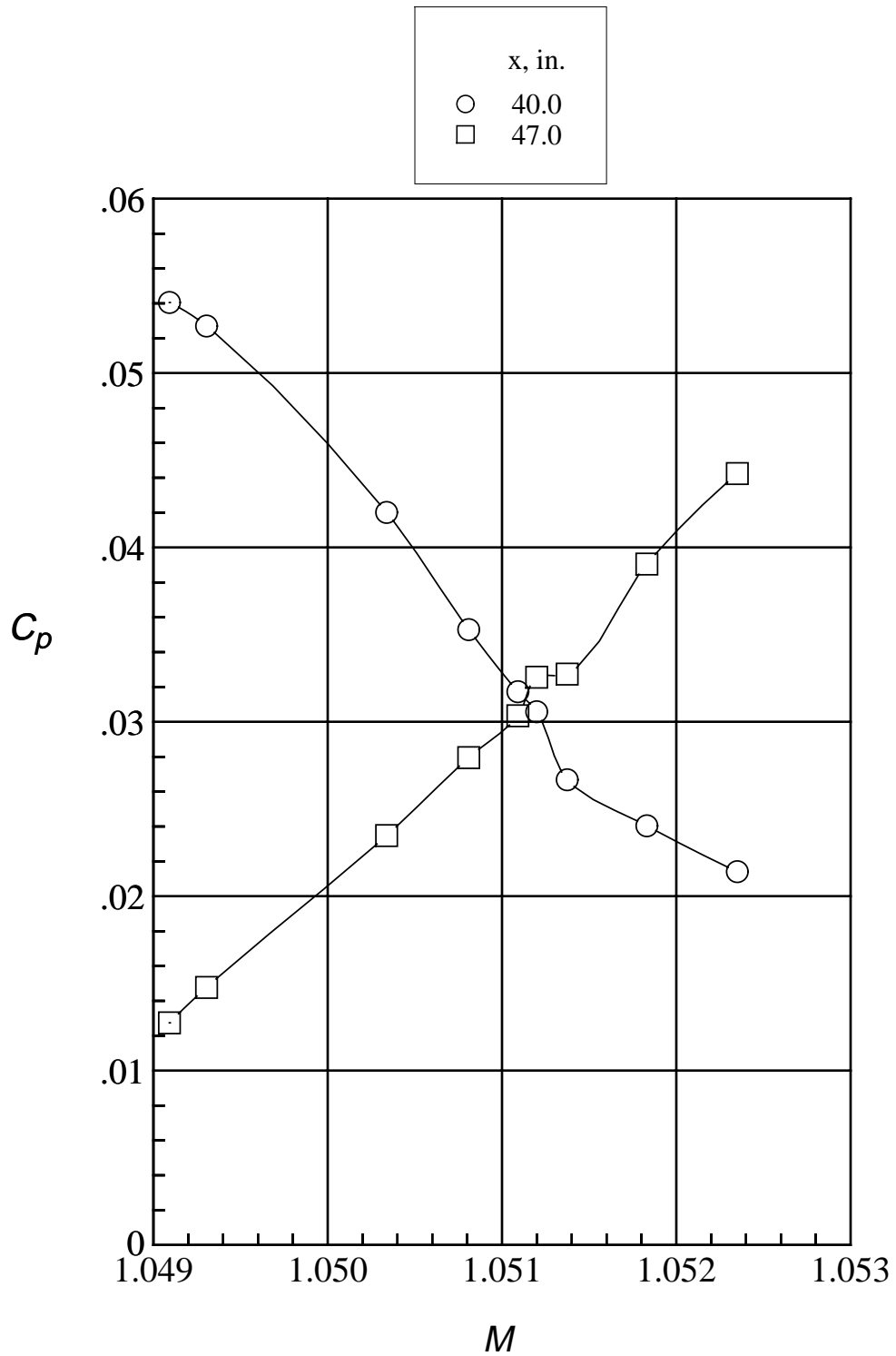


Figure 8. Variation of pressure coefficient with small variations in Mach number at two locations on the model in the vicinity of Mach number 1.05.

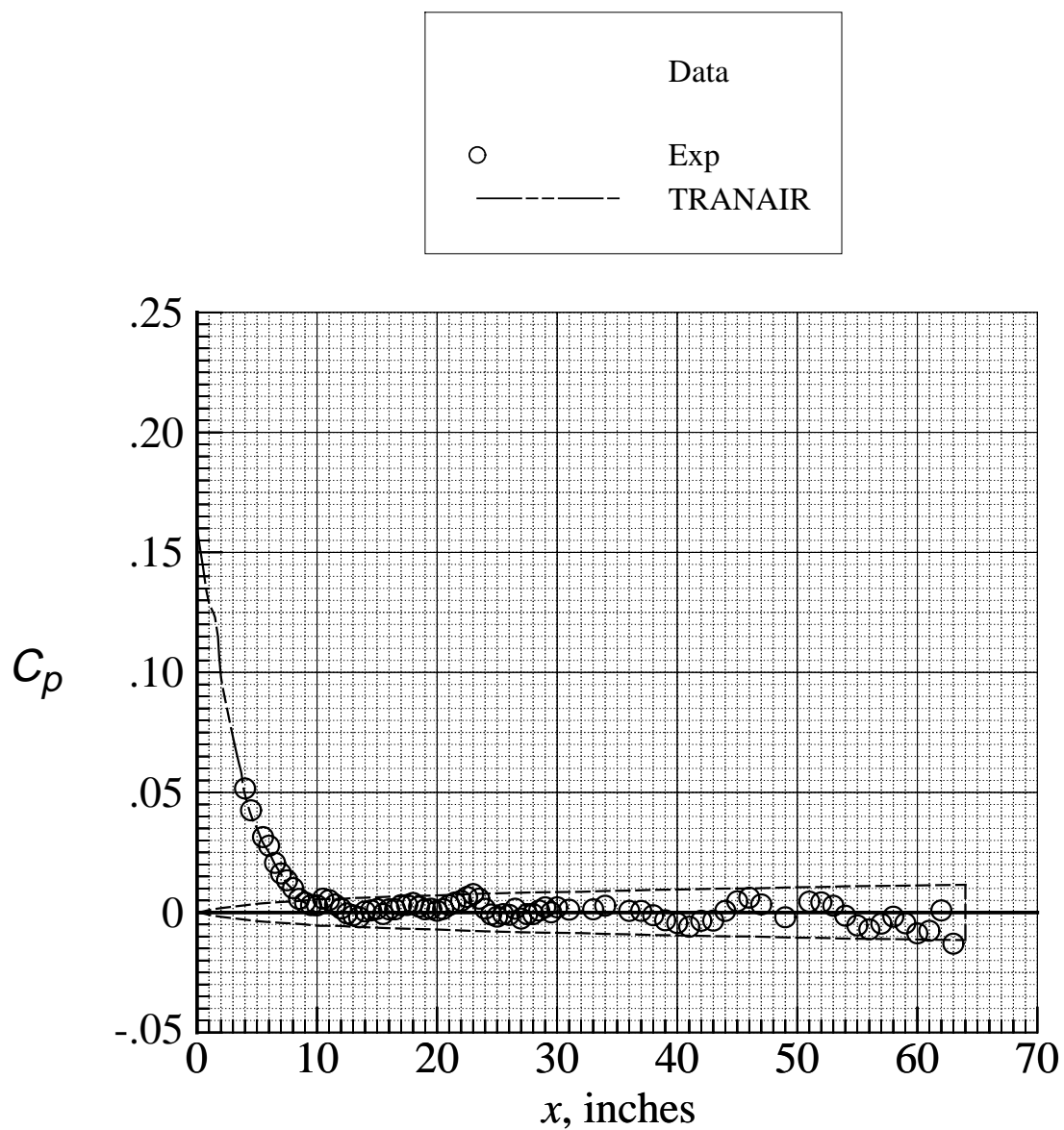


Figure 9. Comparison between measured and calculated pressure distributions at  $\alpha = 0^\circ$  and  $M = 1.25$ .

	Model	Length, in.	Nose half angle, deg	Location	Reference
○	1	96.0	10	Centerline	2
□	2	96.0	20	Centerline	2
◇	3	96.0	Ogive	Centerline	2
△	5	60.0	10	Centerline	2
▴	9	100.3	14	Centerline	2
▢	21	72.0	14	±22 in. off centerline	Unpublished
◻	22	96.0	14	±22 in. off centerline	Unpublished
●	SRB	64.0	-	Centerline	Current

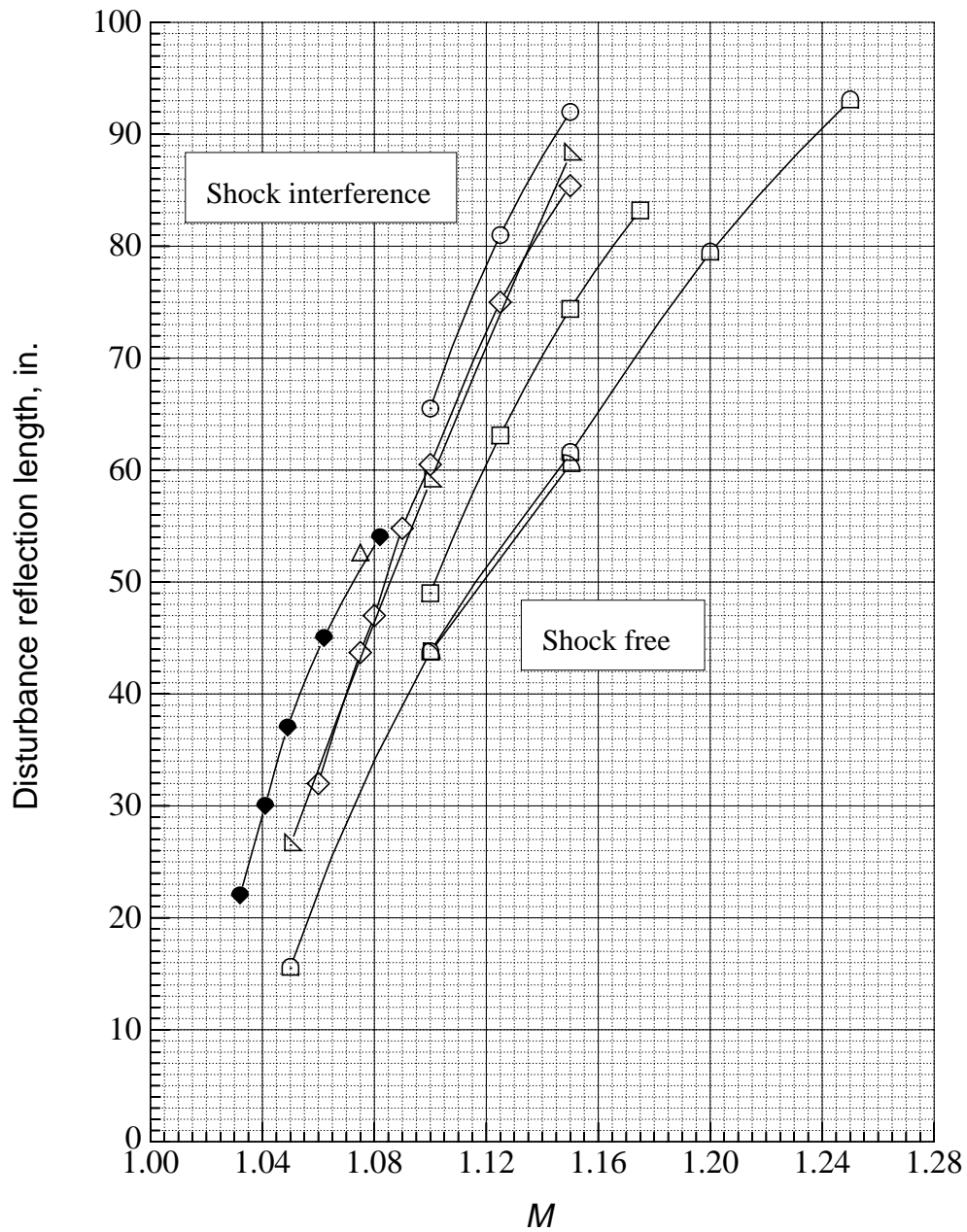


Figure 10. Boundary-reflected-disturbance lengths measured in the Langley 16-Foot Transonic Tunnel for nose originated shocks.